www.nature.com/cmi

ARTICLE

Tubulointerstitial nephritis antigen-like 1 is a novel matricellular protein that promotes gastric bacterial colonization and gastritis in the setting of *Helicobacter pylori* infection

Yongsheng Teng[1,2,10], Rui Xie[3,10], Jingyu Xu[3,10], Pan Wang[1,2], Wanyan Chen[1], Zhiguo Shan[4], Zongbao Yan[4], Fangyuan Mao[1], Ping Cheng[1], Liusheng Peng[1], Jinyu Zhang[1], Wenqing Tian[5], Shiming Yang[6], Yongliang Zhao[4], Weisan Chen[7], Quanming Zou[1]✉ and Yuan Zhuang[8,9]✉

The interaction between the gastric epithelium and immune cells plays key roles in *H. pylori*-associated pathology. Here, we demonstrate a procolonization and proinflammatory role of tubulointerstitial nephritis antigen-like 1 (TINAGL1), a newly discovered matricellular protein, in *H. pylori* infection. Increased TINAGL1 production by gastric epithelial cells (GECs) in the infected gastric mucosa was synergistically induced by *H. pylori* and IL-1β via the ERK-SP1 pathway in a *cagA*-dependent manner. Elevated human gastric TINAGL1 correlated with *H. pylori* colonization and the severity of gastritis, and mouse TINAGL1 derived from non-bone marrow-derived cells promoted bacterial colonization and inflammation. Importantly, *H. pylori* colonization and inflammation were attenuated in *Tinagl1*$^{-/-}$ and *Tinagl1*$^{\Delta GEC}$ mice and were increased in mice injected with mouse TINAGL1. Mechanistically, TINAGL1 suppressed CCL21 expression and promoted CCL2 production in GECs by directly binding to integrin α5β1 to inhibit ERK and activate the NF-κB pathway, respectively, which not only led to decreased gastric influx of moDCs via CCL21-CCR7-dependent migration and, as a direct consequence, reduced the bacterial clearance capacity of the *H. pylori*-specific Th1 response, thereby promoting *H. pylori* colonization, but also resulted in increased gastric influx of Ly6C^{high} monocytes via CCL2-CCR2-dependent migration. In turn, TINAGL1 induced the production of the proinflammatory protein S100A11 by Ly6C^{high} monocytes, promoting *H. pylori*-associated gastritis. In summary, we identified a model in which TINAGL1 collectively ensures *H. pylori* persistence and promotes gastritis.

Keywords: *Helicobacter pylori*; TINAGL1; Colonization; Gastritis

Cellular & Molecular Immunology (2023) 20:924–940; https://doi.org/10.1038/s41423-023-01055-4

INTRODUCTION

Helicobacter pylori (*H. pylori*) is a human pathogen that has infected nearly half of the world's population [1, 2]. Infection with *H. pylori* is frequently associated with chronic gastritis and can even lead to gastric ulcers and gastric cancer [3, 4]. Although the persistent colonization of *H. pylori* and the development of *H. pylori*-associated gastritis in the gastric mucosa remain poorly understood, it is believed that the *H. pylori*-induced interaction between the gastric epithelium and immune cells is a key contributing factor [5, 6]. Gastric epithelial cells (GECs) are the first cells contacted by *H. pylori* in the gastric mucosa. GECs are not only modulated by *H. pylori* but also produce factors that selectively attract immune cells to mount an inflammatory response [7, 8]. Among the many factors secreted by GECs in response to *H. pylori* infection are extracellular matrix (ECM) proteins.

Matricellular proteins are a class of ECM proteins that do not contribute directly to the formation of structural elements but serve to modulate cell function and regulate inflammation through direct binding to other matrix proteins as well as specific surface receptors [9, 10]. Tubulointerstitial nephritis antigen-like 1 (TINAGL1) is a newly discovered matricellular protein [11] and has been proposed to both protect against cancer and contribute to pathological abnormalities in tumors. In triple-negative breast cancer (TNBC), TINAGL1 plays roles in suppressing tumor progression and metastasis, and elevated TINAGL1 protein levels

[1]Department of Microbiology and Biochemical Pharmacy, College of Pharmacy and Laboratory Medicine, Third Military Medical University, Chongqing, China. [2]The 940th Hospital of Joint Logistics Support Force of PLA, Lanzhou, China. [3]The Collaborative Innovation Center of Tissue Damage Repair and Regeneration Medicine of Zunyi Medical University, Zunyi, Guizhou, China. [4]Department of General Surgery and Center of Minimal Invasive Gastrointestinal Surgery, Southwest Hospital, Third Military Medical University, Chongqing, China. [5]Department of Gastroenterology, Chongqing University Cancer Hospital, Chongqing, China. [6]Department of Gastroenterology, XinQiao Hospital, Third Military Medical University, Chongqing, China. [7]La Trobe Institute of Molecular Science, La Trobe University, Bundoora, VIC, Australia. [8]Department of Gastroenterology, Affiliated Hospital of Southwest Medical University, Luzhou, Sichuan, China. [9]National Engineering Research Center of Immunological Products, Third Military Medical University, Chongqing, China. [10]These authors contributed equally: Yongsheng Teng, Rui Xie, Jingyu Xu. ✉email: qmzou@tmmu.edu.cn; yuanzhuang1983@yahoo.com

Received: 2 February 2023 Accepted: 29 May 2023
Published online: 19 June 2023

are associated with good prognosis [12]. In contrast, TINAGL1 upregulation in human hepatocellular carcinoma (HCC) is associated with poor prognosis, as TINAGL1 mechanistically promotes hepatocyte carcinogenesis [13]. To date, there have been no reports on the function of TINAGL1 in infectious diseases, and virtually nothing is known about the regulation, function, and clinical relevance of TINAGL1 during *H. pylori* infection in either humans or mice.

In the current study, we demonstrated, for the first time, a procolonization and proinflammatory role of TINAGL1 in the setting of *H. pylori* infection. Increased TINAGL1 expression was detected in the gastric mucosa of *H. pylori*-infected human patients and mice, and TINAGL1 expression is synergistically induced in GECs by *H. pylori* infection and interleukin (IL)-1β via the extracellular signal-regulated kinase (ERK)-specificity protein 1 (SP1) pathway. We further demonstrated that on the one hand, TINAGL1 directly binds to integrin α5β1 on GECs to suppress CCL21 production by inhibiting ERK, which leads to decreased gastric influx of monocyte-derived dendritic cells (moDCs) via CCL21-CCR7-dependent migration and, as a direct consequence, reduces the bacterial clearance capacity of the *H. pylori*-specific Th1 response, leading to increased *H. pylori* colonization; on the other hand, TINAGL1 promotes CCL2 production by activating nuclear factor κB (NF-κB), which results in increased gastric influx of Ly6C^{high} monocytes via CCL2-CCR2-dependent migration. Furthermore, upon TINAGL1 stimulation, Ly6C^{high} monocytes produce the pro-inflammatory protein S100A11 to promote *H. pylori*-associated gastritis. Collectively, these data highlight a pathological role for TINAGL1 in persistent *H. pylori* infection-induced clinical gastritis.

RESULTS

TINAGL1 expression is increased in the gastric mucosa of *H. pylori*-infected human patients and mice

To evaluate the potential role of TINAGL1 in *H. pylori* infection, we first compared the expression profiles of matricellular proteins in the human gastric mucosa of *H. pylori*-infected and uninfected donors. Among these proteins, *TINAGL1* exhibited the greatest increase in expression in the gastric mucosa of donors infected with *H. pylori* compared to the paired uninfected counterparts (Supplementary Fig. S1). We then analyzed the expression of *TINAGL1* in the primary gastric mucosa of 81 *H. pylori*-infected and 36 uninfected human patients and confirmed that, compared to that in uninfected donors, *TINAGL1* expression was higher in the gastric mucosa of *H. pylori*-infected patients (Fig. 1A); we further found that *TINAGL1* expression was positively correlated with *H. pylori* colonization (Fig. 1B), suggesting that *H. pylori* may induce TINAGL1 expression. Furthermore, higher *TINAGL1* expression was strongly associated with more severe gastritis in the gastric mucosa of *H. pylori*-infected patients (Fig. 1C), suggesting that TINAGL1 may promote inflammation during *H. pylori* infection. Similar observations were made when TINAGL1 protein expression in these samples was analyzed by ELISA (Fig. 1D–F).

As *cagA* is strongly associated with the development of gastritis [14], we next investigated the relationship between *cagA* and TINAGL1 and found that both *TINAGL1* gene (Fig. 1G) and TINAGL1 protein (Fig. 1H) expression were significantly higher in *cagA*-positive patients than in *cagA*-negative individuals. Consistent with our findings in humans, *Tinagl1* expression was also detected in WT *H. pylori*-infected but not *ΔcagA H. pylori*-infected mice, reaching a peak 14 weeks post infection (p.i.) (Fig. 1I), indicating a key role for *cagA* in inducing TINAGL1 expression during *H. pylori* infection in vivo. Furthermore, western blot analysis (Fig. 1J) showed that the level of the TINAGL1 protein was higher in the gastric mucosa of *cagA*-positive *H. pylori*-infected patients and WT *H. pylori*-infected mice than in uninfected or *cagA*-negative patients and *ΔcagA H. pylori*-infected mice, respectively. Furthermore, *TINAGL1* expression and the TINAGL1 protein abundance were increased significantly in human gastric mucosa infected with WT *H. pylori* ex vivo compared to those in uninfected samples and samples infected with *ΔcagA H. pylori* (Fig. 1K). Similar observations were made when analyzing *Tinagl1* gene and TINAGL1 protein expression in mouse gastric mucosa infected with WT or *ΔcagA H. pylori* ex vivo (Fig. 1L). Collectively, these data demonstrate that TINAGL1 expression is increased in the *H. pylori*-infected gastric mucosa of human patients and mice.

Gastric epithelial cells infected with *H. pylori* produce TINAGL1

Gastric epithelial cells (GECs) are known to be the first cell type in the gastric mucosa contacted during *H. pylori* infection [14]. We therefore analyzed *Tinagl1* expression using public microarray data from the Gene Expression Omnibus (GEO) database, which contains expression data collected from a mouse gastric epithelial progenitor-derived cell line infected with two *H. pylori* strains (the chronic atrophic gastritis (ChAG)-associated Kx1 and the gastric cancer-associated Kx2 strains) [15]. Our analysis showed that Kx1 and Kx2 both significantly induced *Tinagl1* expression (Supplementary Fig. 2A).

Next, we demonstrated that *H. pylori*-infected AGS cells exhibited increased *TINAGL1* expression and TINAGL1 production in a time-dependent (Fig. 2A) and infection dose-dependent (Fig. 2B) manner. Notably, compared to uninfected or *ΔcagA H. pylori*-infected AGS cells, WT *H. pylori*-infected AGS cells also exhibited a potent increase in *TINAGL1* expression and TINAGL1 production (Fig. 2C). Similar observations were made in other human GEC lines (Supplementary Fig. 2B, C). To explore the nature of TINAGL1 induction more closely, we performed transwell assays and found that bacterium-cell contact was necessary for the induction of *TINAGL1* expression in AGS cells infected with *H. pylori* (Supplementary Fig. 2D). Furthermore, we confirmed that in human primary GECs (Fig. 2D–F) as well as mouse primary GECs (Fig. 2G–I), *H. pylori* infection induced increases in *TINAGL1*/*Tinagl1* expression and TINAGL1 production in a manner dependent on *cagA*, time and infection dose. Taken together, our data demonstrate that *H. pylori* induces TINAGL1 production in GECs.

To explore the underlying mechanism of TINAGL1 induction in GECs by *H. pylori*, we performed signaling pathway blockade experiments, and the results showed that only blocking signal transduction in the ERK pathway with the inhibitor U0126 effectively decreased *TINAGL1* expression in WT *H. pylori*-infected AGS cells (Supplementary Fig. 2E). Furthermore, TINAGL1 and ERK1/2, a direct downstream substrate in the ERK pathway, exhibited predominant increases in expression and phosphorylation in AGS cells after infection with WT *H. pylori*, and these increases were abolished when the cells were pretreated with U0126 (Fig. 2J). To further investigate how *H. pylori* induces *TINAGL1* gene transcription, we constructed a series of *TINAGL1*-luc promoter constructs of varying lengths (−2000/0, −1000/0, −500/0, −260/0) and performed luciferase reporter assays; the results showed that only the shortest *TINAGL1* promoter (−260/0) mediated transcriptional responsiveness to *H. pylori* (Supplementary Fig. 2F). Furthermore, compared to *ΔcagA H. pylori* infection, infection with WT *H. pylori* significantly enhanced this luciferase activity, and pretreatment with U0126 abrogated the increase in luciferase activity induced by WT *H. pylori* (Fig. 2K). The PROMO tool in V.8.3 of TRANSFAC (Beverly, MA, USA) showed that the *TINAGL1* promoter (−260/0) contains three SP1 binding sites (Supplementary Fig. 2G). Subsequently, the chromatin immunoprecipitation (ChIP) assay results showed that, compared to no infection or *ΔcagA H. pylori* infection, WT *H. pylori* infection significantly increased SP1 binding to the *TINAGL1* promoter in AGS cells, and this increase was abolished when the cells were pretreated with U0126 (Fig. 2L). Taken together, these findings clearly demonstrate that *cagA*-mediated ERK signaling pathway activation modulates SP1-mediated transcriptional regulation of *TINAGL1* expression in GECs during *H. pylori* infection.

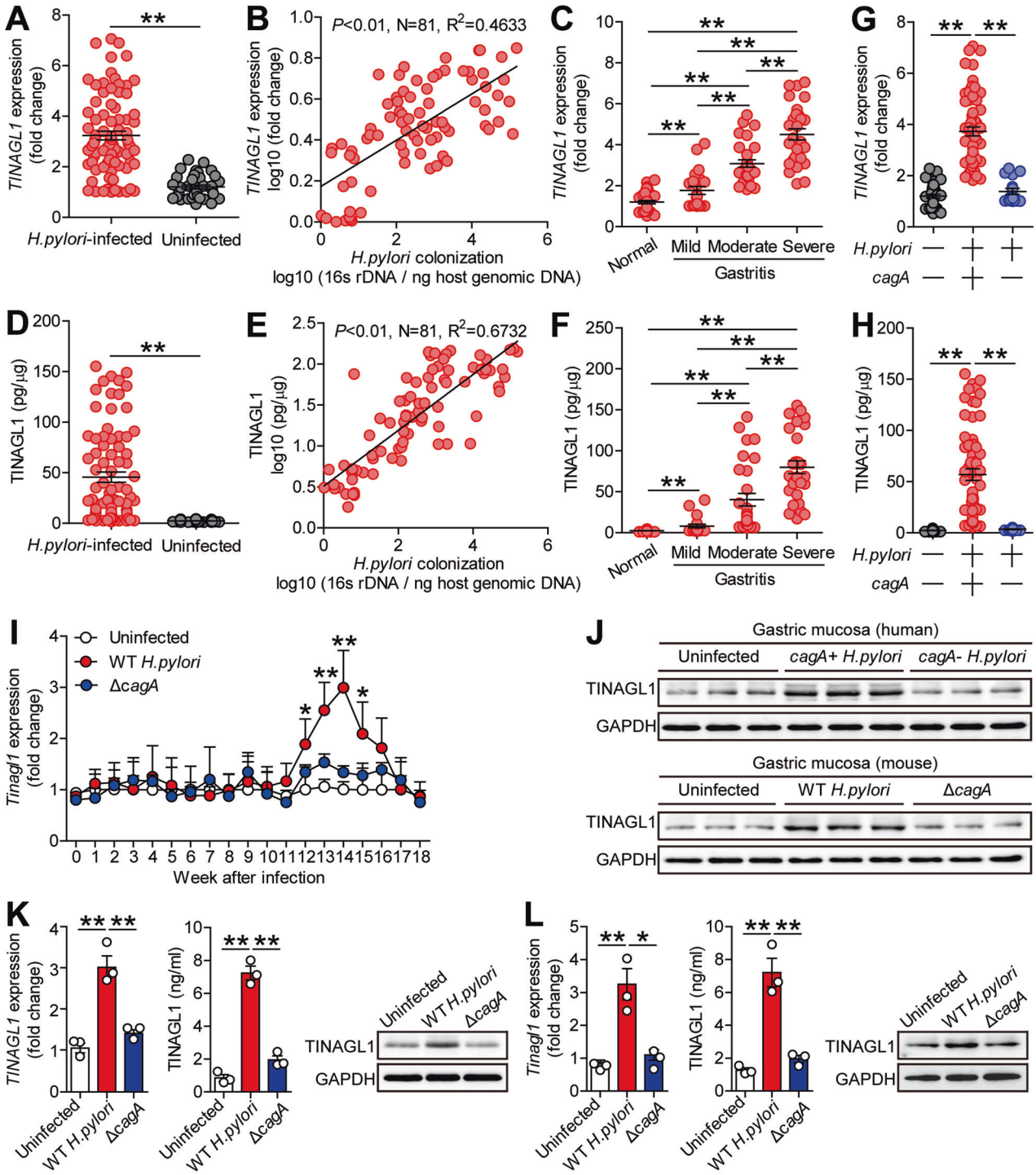

Fig. 1 TINAGL1 is increased in the gastric mucosa of *H. pylori*-infected human patients and mice. *TINAGL1* expression (**A**) and TINAGL1 protein production (**D**) in the gastric mucosa of *H. pylori*-infected ($n = 81$) and uninfected donors ($n = 36$) were compared. The correlations between *TINAGL1* expression (**B**) and TINAGL1 protein production (**E**) and *H. pylori* colonization in the gastric mucosa of *H. pylori*-infected patients were analyzed. *TINAGL1* expression (**C**) and TINAGL1 protein production (**F**) in the gastric mucosa of *H. pylori*-infected patients with mild ($n = 22$), moderate ($n = 30$), and severe ($n = 29$) inflammation and uninfected donors with normal gastric histology ($n = 36$) were compared. *TINAGL1* expression (**G**) and TINAGL1 protein production (**H**) in the gastric mucosa of $cagA^+$ *H. pylori*-infected ($n = 64$), $cagA^-$ *H. pylori*-infected ($n = 17$), and uninfected ($n = 36$) donors was compared. **I** Dynamic changes in *Tinagl1* expression in the gastric mucosa of WT *H. pylori*-infected, *ΔcagA H. pylori*-infected, and uninfected mice. $n = 5$ mice per group per time point in (**I**). **J** TINAGL1 protein production in the gastric mucosa of $cagA^+$ *H. pylori*-infected, $cagA^-$ *H. pylori*-infected, and uninfected donors and in the gastric mucosa of WT *H. pylori*-infected, *ΔcagA H. pylori*-infected, and uninfected mice 14 weeks p.i. was analyzed by western blotting. **K**, **L** *TINAGL1*/*Tinagl1* expression and TINAGL1 protein production in primary gastric mucosa from uninfected human donors/mice infected with WT *H. pylori* or *ΔcagA H. pylori* ex vivo were analyzed by real-time PCR, ELISA and western blotting ($n = 3$). Data are representative of two independent experiments. Data are shown as the means ± SEMs and were analyzed by Student's *t* test, the Mann–Whitney *U* test or one-way ANOVA. Western blotting was performed in parallel and simultaneously. $^*P < 0.05$, $^{**}P < 0.01$ between the groups connected by horizontal lines or compared with uninfected mice

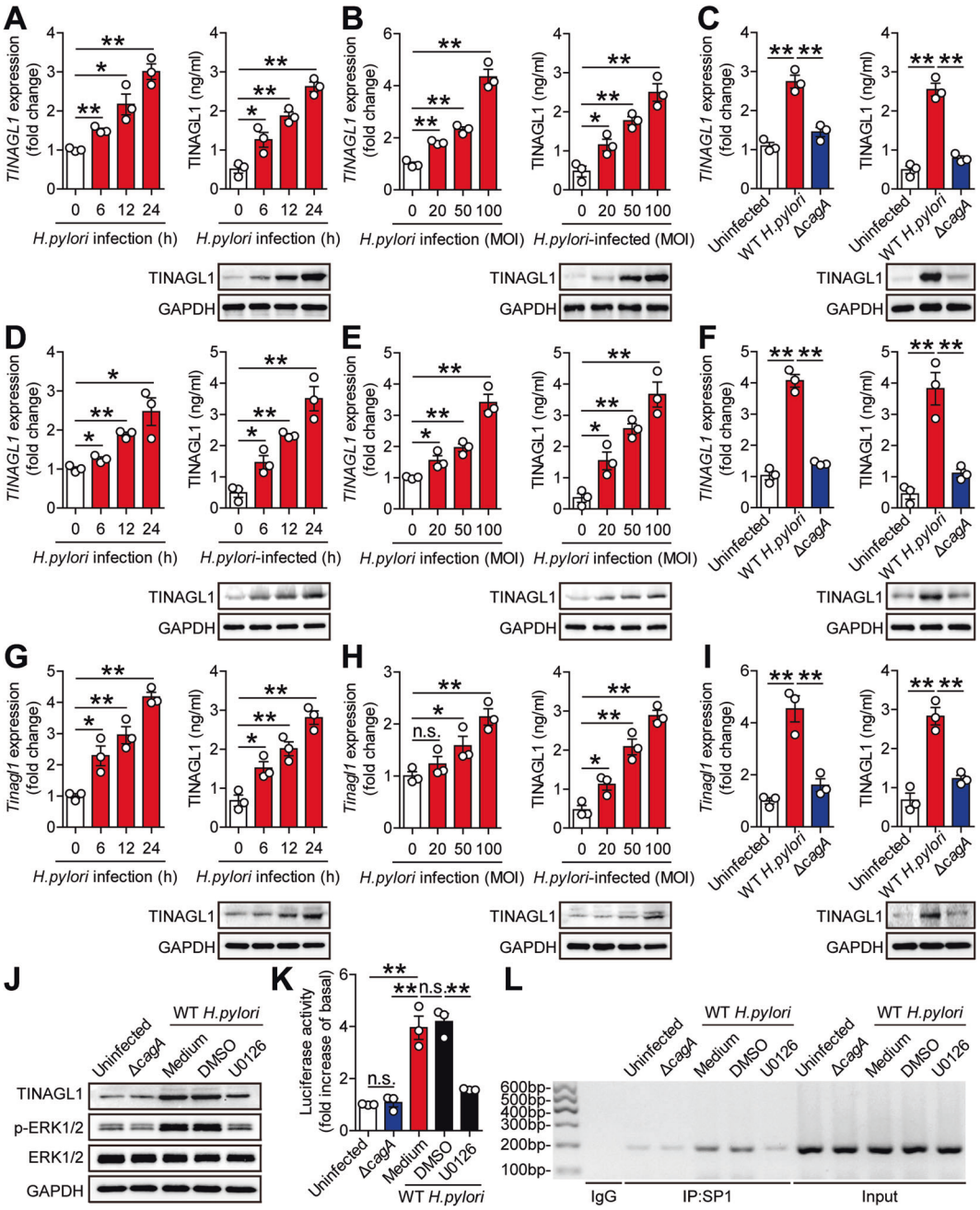

Fig. 2 *H. pylori* stimulates TINAGL1 production in gastric epithelial cells (GECs). *TINAGL1* expression and TINAGL1 protein production in WT *H. pylori*-infected and uninfected AGS cells at different time points (MOI = 100) (**A**) or after infection at different MOIs (24 h) (**B**) were analyzed by real-time PCR, ELISA and western blotting ($n = 3$). (**C**) *TINAGL1* expression and TINAGL1 protein production in WT *H. pylori*-infected, *ΔcagA H. pylori*-infected, and uninfected AGS cells (MOI = 100, 24 h) were analyzed by real-time PCR, ELISA and western blotting ($n = 3$). *TINAGL1* expression and TINAGL1 protein production in WT *H. pylori*-infected and uninfected human primary GECs at different time points (MOI = 100) (**D**) or after infection at different MOIs (24 h) (**E**) were analyzed by real-time PCR, ELISA and western blotting ($n = 3$). **F** *TINAGL1* expression and TINAGL1 protein production in WT *H. pylori*-infected, *ΔcagA H. pylori*-infected, and uninfected human primary GECs (MOI = 100, 24 h) were analyzed by real-time PCR, ELISA and western blotting ($n = 3$). *Tinagl1* expression and TINAGL1 protein production in WT *H. pylori*-infected and uninfected mouse primary GECs at different time points (MOI = 100) (**G**) or after infection at different MOIs (24 h) (**H**) were analyzed by real-time PCR, ELISA and western blotting ($n = 3$). **I** *Tinagl1* expression and TINAGL1 protein production in WT *H. pylori*-infected, *ΔcagA H. pylori*-infected, and uninfected mouse primary GECs (MOI = 100, 24 h) were analyzed by real-time PCR, ELISA and western blotting ($n = 3$). **J** AGS cells were pretreated with U0126 and then infected with WT *H. pylori* or *ΔcagA H. pylori* (MOI = 100) for 24 h. TINAGL1, ERK1/2 and p-ERK1/2 protein levels were measured by western blotting. **K** AGS cells were transfected with luciferase reporter constructs containing the *TINAGL1*-luc promoter for 4 h. Luciferase activity was measured to assess promoter activity after WT *H. pylori* (with or without U0126 pretreatment) or *ΔcagA H. pylori* infection (MOI = 100) for 24 h. **L** Representative data from AGS cells infected with WT *H. pylori* (with or without U0126 pretreatment) or *ΔcagA H. pylori* and subjected to ChIP followed by regular PCR with primers designed to target the SP1 binding site in the *TINAGL1* promoter region. Data are representative of two independent experiments. Data are shown as the means ± SEMs and were analyzed by one-way ANOVA. Western blotting was performed in parallel and simultaneously. $^*P < 0.05$, $^{**}P < 0.01$, n.s. $P > 0.05$ between the groups connected by horizontal lines

H. pylori and IL-1β synergistically induce TINAGL1

Previous data have shown that helper T (Th) cell responses such as the Th1 [16], Th2 [17], Th17 [18] and Th22 [19] responses play critical roles in *H. pylori*-associated pathology. To explore whether cytokines released from these Th cells and cytokines that regulate these Th cells have synergistic effects on inducing TINAGL1 during *H. pylori* infection, we first infected AGS cells with *H. pylori* in the presence or absence of IFN-γ, IL-4, IL-17A, IL-22, IL-12, IL-6, IL-1β or IL-23 in vitro and found that only IL-1β exerted a synergistic effect on *TINAGL1* expression (Fig. 3A; Supplementary Fig. 3) and TINAGL1 production (Fig. 3A). Similar observations were made using human primary GECs (Fig. 3B) as well as mouse primary GECs (Fig. 3C) infected with *H. pylori* in the presence or absence of IL-1β. Furthermore, *TINAGL1*/*Tinagl1* expression was found to be positively correlated with *IL1B*/*Il1b* expression in the gastric mucosa of *H. pylori*-infected human patients and mice (Fig. 3D). The results suggest that *H. pylori* and IL-1β synergistically induce TINAGL1.

To further explore whether the ERK signaling pathway might operate similarly in the induction of TINAGL1 in GECs by *H. pylori* and IL-1β, we first pretreated AGS cells with U0126 or anti-IL-1β Abs and then infected them with *H. pylori* and treated them with IL-1β. The results showed that blockade of signal transduction in the ERK pathway or treatment with IL-1β effectively decreased *TINAGL1* expression, TINAGL1 production and ERK1/2 phosphorylation (Fig. 3E). Moreover, blockade of signal transduction in the ERK pathway or treatment with IL-1β also efficiently inhibited *H. pylori*- and IL-1β-induced *TINAGL1* transcriptional activity (Fig. 3F) and SP1 binding to the *TINAGL1* promoter (Fig. 3G) in AGS cells. Taken together, these findings suggest that the induction of TINAGL1 in *H. pylori*-infected GECs can be synergistically enhanced by IL-1β via activation of the ERK-SP1 signaling pathway.

Given the critical importance of IL-1 receptor 1 (IL-1R1) in IL-1β signaling [20], we sought to evaluate IL-1R1 expression during *H. pylori* infection. Indeed, *H. pylori*-infected AGS cells exhibited increased IL-1R1 expression in a time-dependent and infection dose-dependent manner (Fig. 3H). Similar observations were made in human primary GECs as well as mouse primary GECs infected with *H. pylori* (Fig. 3I). Furthermore, the induction of *TINAGL1*/*Tinagl1* expression and TINAGL1 production by *H. pylori* and IL-1β was attenuated when the IL-1β-IL-1R1 interaction was abolished in AGS cells by treatment with *IL1R1* siRNA (Fig. 3J) and in primary GECs from *Il1r1*$^{-/-}$ mice (Fig. 3K). Collectively, these results suggest that *H. pylori* infection induces IL-1R1 expression on GECs, which enhances the synergistic effects of *H. pylori* and IL-1β on TINAGL1 induction.

TINAGL1 increases the bacterial burden, inflammation and Ly6C^{high} monocyte accumulation but decreases moDC infiltration in the gastric mucosa during *H. pylori* infection

To evaluate the possible biological effects of TINAGL1 in *H. pylori*-associated pathogenesis in vivo, we conducted a series of loss- and gain-of-function experiments involving TINAGL1 and compared the levels of bacterial colonization in gastric mucosa 14 weeks p.i. We found that the lack of TINAGL1 in *Tinagl1*$^{-/-}$ mice (Supplementary Fig. 4) led to reduced gastric *H. pylori* colonization compared to that in WT mice; conversely, injection of TINAGL1 into these mice significantly increased gastric *H. pylori* colonization (Fig. 4A). We next generated reciprocal bone marrow chimeras (BMs) between WT and *Tinagl1*$^{-/-}$ mice and found that TINAGL1 produced by non-BM-derived cells was responsible for gastric *H. pylori* colonization in this model (Fig. 4A). These data suggest that TINAGL1 affects the bacterial burden during *H. pylori* infection in vivo.

As *H. pylori* induces TINAGL1 production in GECs (Fig. 2), we next tried to evaluate the potential role of GEC-derived TINAGL1 in *H. pylori* infection. Parietal cells expressing the unique enzyme hydrogen potassium ATPase (H^+/K^+ ATPase) are one of the largest GEC subsets, and the promoter of the β-subunit of the H^+/K^+ ATPase (*Atp4b*) has been used to drive gene expression in parietal cells [21]. Interestingly, within the gastric mucosa of *H. pylori*-infected human patients and mice, TINAGL1 was detected almost exclusively in H^+/K^+ ATPase+ parietal cells, suggesting that parietal cells are the source GECs that produce TINAGL1 in the gastric mucosa during *H. pylori* infection (Supplementary Fig. 4C). Thus, we generated mice with GEC-specific *Tinagl1* knockout (*Atp4b-Cre;Tinagl1*$^{flox/flox}$, also called *Tinagl1*$^{\Delta GEC}$) and found that gastric *H. pylori* colonization was significantly decreased in *Tinagl1*$^{\Delta GEC}$ mice compared to their TINAGL1$^{flox/flox}$ littermates (Fig. 4A). These data suggest that TINAGL1 affects the bacterial burden during *H. pylori* infection in vivo.

We next evaluated the inflammatory response in the gastric mucosa 14 weeks p.i. Compared with WT mice, *Tinagl1*$^{-/-}$ mice showed significantly less inflammation in the gastric mucosa, and injection of TINAGL1 significantly increased gastric inflammation (Fig. 4B; Supplementary Fig. 5A). Again, TINAGL1 produced by non-BM-derived cells was responsible for gastric inflammation in this model (Fig. 4B; Supplementary Fig. 5A). Importantly, gastric inflammation was significantly decreased in *Tinagl1*$^{\Delta GEC}$ mice compared to their *Tinagl1*$^{flox/flox}$ littermates (Fig. 4B; Supplementary Fig. 5A). Collectively, these results suggest that TINAGL1 promotes inflammation during *H. pylori* infection in vivo.

In addition to GECs, monocytes [22], dendritic cells (DCs) [23, 24], macrophages [25] and neutrophils [26] are the cells that can come into direct contact with *H. pylori*. To investigate whether increased TINAGL1 production regulates the infiltration of these cells and their subsets into the gastric mucosa during *H. pylori* infection, stomach cell suspensions obtained after enzymatic digestion were analyzed by multicolor flow cytometry. After gating on CD45$^+$ cells and excluding cells expressing CD90 (T cells), CD19 (B cells), CD49b (NK cells) or Siglec-F (eosinophils), a sequential gating strategy based on the differential expression of Ly6G, CD11b, CD64, Ly6C, MHCII and CD11c allowed the characterization of tissue-resident macrophages, neutrophils, Ly6C^{low} monocytes, Ly6C^{high} monocytes, MHCII$^+$ monocytes, monocyte-derived DCs (moDCs), immature moDCs (i-moDCs) and conventional DCs (cDCs) (Supplementary Fig. 5B). Comparison of the percentages of these cells in the gastric mucosa 14 weeks p.i. showed that the lack of TINAGL1 in *Tinagl1*$^{-/-}$ mice led to a reduction in the population of gastric Ly6C^{high} monocytes (Fig. 4C–G; Supplementary Fig. 5C, D) but not blood (Supplementary Fig. 6), spleen (Supplementary Fig. 7) or BM (Supplementary Fig. 8) Ly6C^{high} monocytes; however, *Tinagl1*$^{-/-}$ mice showed an increased population of only gastric Ly6C^{high} monocytes (Fig. 4C–G; Supplementary Fig. 5C, D) and not blood (Supplementary Fig. 6), spleen (Supplementary Fig. 7) or BM (Supplementary Fig. 8) moDCs. Furthermore, injection of TINAGL1 significantly increased the population of gastric Ly6C^{high} monocytes and decreased the population of gastric moDCs (Fig. 4C–G). These results were also confirmed by our BM chimera experiments, in which non-BM-derived TINAGL1 was found to be largely responsible for the increased Ly6C^{high} monocyte accumulation and decreased moDC infiltration in the gastric mucosa during *H. pylori* infection (Fig. 4C–G). Importantly, decreased Ly6C^{high} monocyte and increased moDC populations were found in *Tinagl1*$^{\Delta GEC}$ mice compared to their *Tinagl1*$^{flox/flox}$ littermates (Fig. 4C–G). Taken together, our data demonstrate that TINAGL1 plays an essential role in increasing the bacterial burden, inflammation and Ly6C^{high} monocyte accumulation and decreasing moDC infiltration in the gastric mucosa during *H. pylori* infection.

TINAGL1 suppresses CCL21 production and promotes CCL2 production in GECs by directly binding to integrin α5β1 to inhibit the ERK pathway and activate the NF-κB pathway, respectively

We next investigated the underlying mechanism by which TINAGL1 suppresses moDC but promotes Ly6C^{high} monocyte

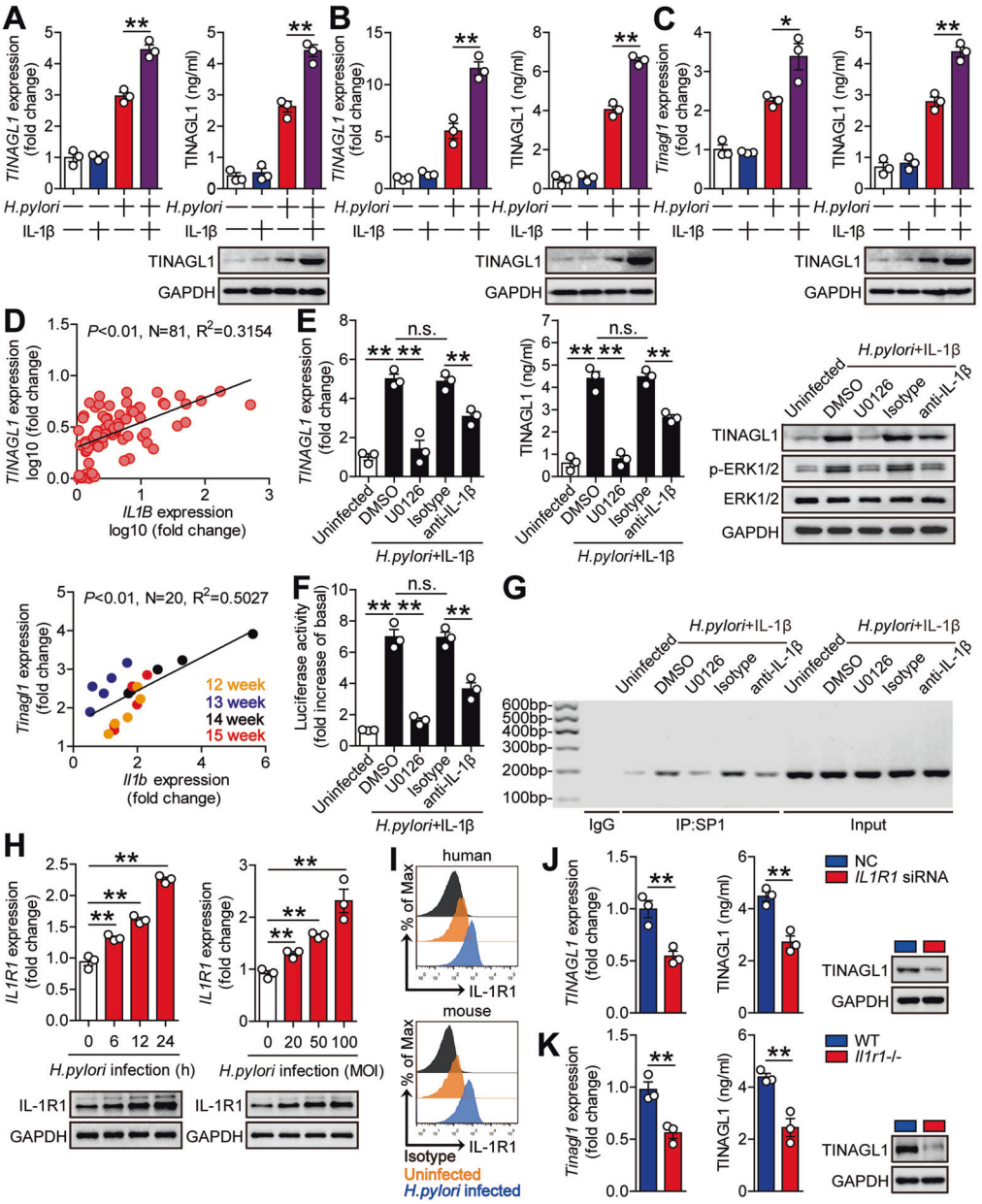

Fig. 3 *H. pylori* and IL-1β synergistically induce TINAGL1. *TINAGL1*/*Tinagl1* expression and TINAGL1 protein production in AGS cells (**A**), human primary GECs (**B**) and mouse primary GECs (**C**) infected with WT *H. pylori* (MOI = 100) in the presence or absence of IL-1β (100 ng/ml) (24 h) were analyzed by real-time PCR, ELISA and western blotting ($n = 3$). **D** The correlations between *TINAGL1* expression and *IL1B* expression in the gastric mucosa of *H. pylori*-infected patients and between *Tinagl1* expression and *Il1b* expression in the gastric mucosa of *H. pylori*-infected mice 12, 13, 14 and 15 weeks p.i. were analyzed. **E** AGS cells were pretreated with U0126 or anti-IL-1β neutralizing Abs and then infected with WT *H. pylori* (MOI = 100) in the presence of IL-1β (100 ng/ml) for 6 h or 24 h. *TINAGL1* expression and TINAGL1 protein production were analyzed by real-time PCR and ELISA ($n = 3$). TINAGL1, ERK1/2 and p-ERK1/2 protein levels were measured by western blotting. **F** AGS cells were transfected with luciferase reporter constructs containing the *TINAGL1*-luc promoter for 4 h. Luciferase activity was measured to assess promoter activity after WT *H. pylori* (MOI = 100) infection in the presence of IL-1β (100 ng/ml) (with or without pretreatment with U0126 or anti-IL-1β neutralizing Abs) for 24 h. **G** Representative data from AGS cells infected with WT *H. pylori* (MOI = 100) in the presence of IL-1β (100 ng/ml) (with or without pretreatment with U0126 or anti-IL-1β neutralizing Abs) and subjected to ChIP followed by regular PCR with primers designed to target the SP1 binding site in the *TINAGL1* promoter region. **H** *IL-1R1* expression and IL-1R1 protein production in WT *H. pylori*-infected and uninfected AGS cells at different time points (MOI = 100) or after infection at different MOIs (24 h) were analyzed by real-time PCR and western blotting ($n = 3$). **I** IL-1R1 protein expression on WT *H. pylori*-infected human/mouse primary GECs (MOI = 100, 24 h) was analyzed by flow cytometry. *IL-1R1* siRNA- and nonspecific control siRNA (NC)-pretreated AGS cells (**J**) and primary GECs from uninfected $Il1r1^{-/-}$ and WT mice (**K**) were infected with WT *H. pylori* (MOI = 100) in the presence of IL-1β (100 ng/ml) for 24 h. *TINAGL1*/*Tinagl1* expression and TINAGL1 protein production were analyzed by real-time PCR, ELISA and western blotting ($n = 3$). Data are representative of two independent experiments. Data are shown as the means ± SEMs and were analyzed by Student's *t* test, the Mann–Whitney *U* test or one-way ANOVA. Western blotting was performed in parallel and simultaneously. $^*P < 0.05$, $^{**}P < 0.01$, n.s. $P > 0.05$ between the groups connected by horizontal lines

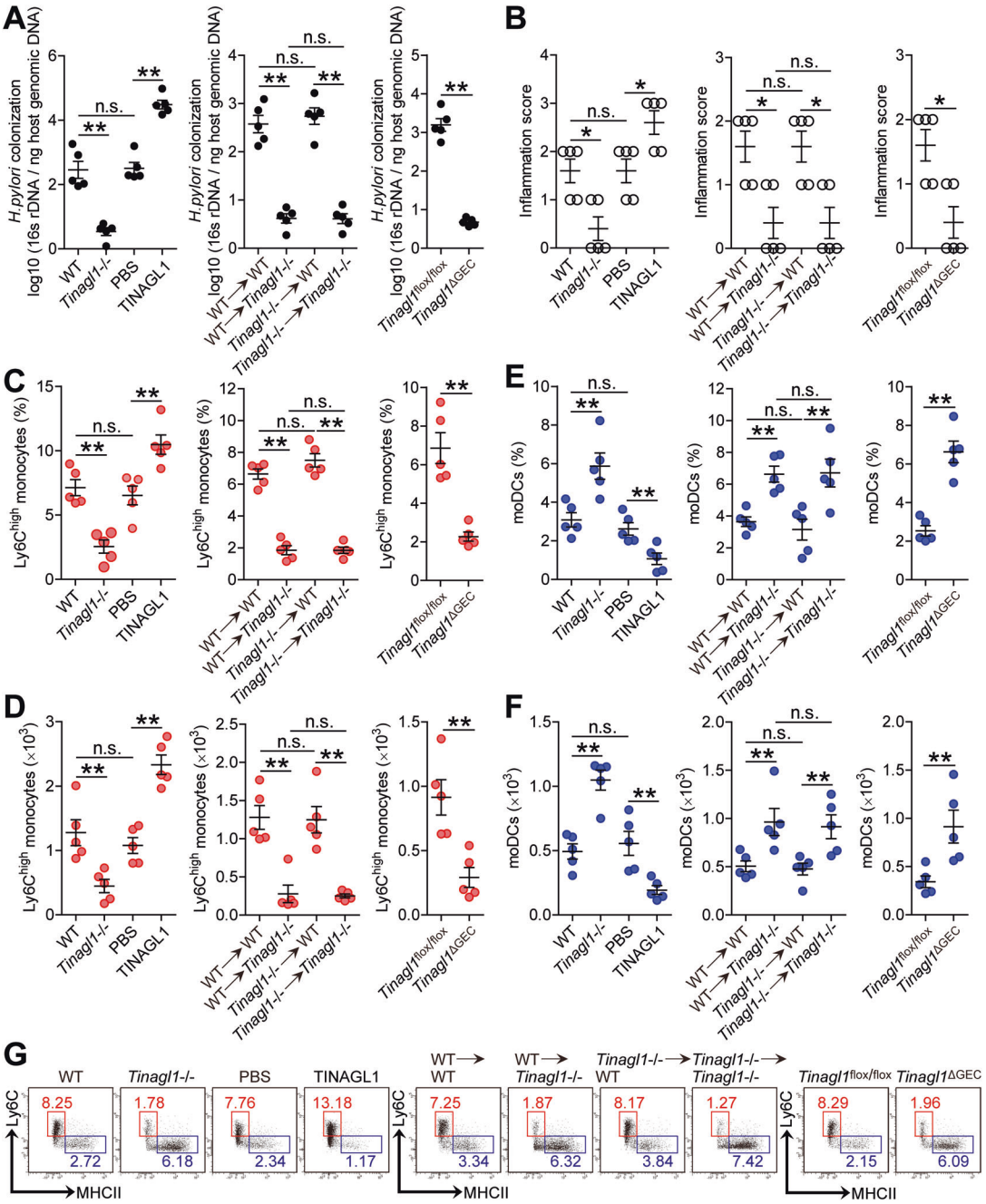

Fig. 4 TINAGL1 increases the bacterial burden, inflammation and Ly6C^{high} monocyte accumulation but decreases moDC accumulation in the gastric mucosa during *H. pylori* infection. Bacterial colonization (**A**) and histological scores of inflammation (**B**) in the gastric mucosa of *H. pylori*-infected WT and *Tinagl1*$^{-/-}$ mice, in the gastric mucosa of WT mice injected with TINAGL1 or PBS control, in the gastric mucosa of *H. pylori*-infected BM chimeric mice, and in the gastric mucosa of *H. pylori*-infected *Tinagl1*$^{flox/flox}$ and *Tinagl1*$^{\Delta GEC}$ mice 14 weeks p.i. were compared ($n = 5$). The Ly6C^{high} monocyte populations in the gastric mucosa of *H. pylori*-infected WT and *Tinagl1*$^{-/-}$ mice and in the gastric mucosa of WT mice injected with TINAGL1 *H. pylori*-infected *Tinagl1*$^{flox/flox}$ and *Tinagl1*$^{\Delta GEC}$ mice 14 weeks p.i. were compared ($n = 5$). The results are expressed as the percentage of Ly6C^{high} monocytes among CD45^{+} cells (**C**) or the number of Ly6C^{high} monocytes per million total cells (**D**) in the gastric mucosa. **E**, **F** The moDC populations in the gastric mucosa of *H. pylori*-infected WT and *Tinagl1*$^{-/-}$ mice, in the gastric mucosa of WT mice injected with TINAGL1 or PBS control, in the gastric mucosa of *H. pylori*-infected BM chimeric mice, and in the gastric mucosa of *H. pylori*-infected *Tinagl1*$^{flox/flox}$ and *Tinagl1*$^{\Delta GEC}$ mice 14 weeks p.i. were compared ($n = 5$). The results are expressed as the percentage of moDCs among CD45^{+} cells (**E**) or the number of moDCs per million total cells (**F**) in the gastric mucosa. **G** Representative dot plots of Ly6C^{high} monocytes and moDCs (defined as described in Supplementary Fig. 5B) in the gastric mucosa of *H. pylori*-infected WT and *Tinagl1*$^{-/-}$ mice, in the gastric mucosa of WT mice injected with TINAGL1 or PBS control, in the gastric mucosa of *H. pylori*-infected BM chimeric mice, and in the gastric mucosa of *H. pylori*-infected *Tinagl1*$^{flox/flox}$ and *Tinagl1*$^{\Delta GEC}$ mice 14 weeks p.i. The red and blue numbers indicate the relative percentages of Ly6C^{high} monocytes and moDCs, respectively, among CD45^{+} cells. Data are representative of two independent experiments. Data are shown as the means ± SEMs and were analyzed by Student's *t* test, the Mann–Whitney *U* test or one-way ANOVA. *$P < 0.05$, **$P < 0.01$, n.s. $P > 0.05$ between the groups connected by horizontal lines

migration to the gastric mucosa during *H. pylori* infection. As chemotaxis plays important roles in myeloid cell migration [27], we investigated the role of TINAGL1 in GEC chemokine production. First, immunoprecipitation (IP) followed by mass spectrometry (MS) was employed to identify potential interacting partners of TINAGL1 (Fig. 5A). Protein network analysis of the proteins identified by MS identified the top ten Gene Ontology (GO) terms in the "Cellular Component" and "Biological Process" categories significantly enriched in the candidate interacting partners (Fig. 5B), with one candidate, integrin β1, overlapping and present in both the GO term "membrane" in the "Cellular Component" category and the GO term "regulation of immune response" in the "Biological Process" category (Fig. 5C). The normalized intensity ratios calculated from the MS spectral counts revealed that integrin β1 was an abundant protein (Supplementary Fig. S9A). Next, we validated the interaction between TINAGL1 and integrin β1 by coimmunoprecipitation experiments using AGS cells stably expressing TINAGL1-Flag (Fig. 5D). As functional complexes, integrins are heterodimers composed of α and β subunits [28]. We further showed that subunit α5 also interacted with TINAGL1 (Fig. 5D). To further confirm whether TINAGL1 colocalizes with integrin α5β1 on the GEC membrane, we incubated AGS cells with TINAGL1 at 4 °C for 3 h. Confocal microscopy using Abs specific to TINAGL1 and integrin α5 or integrin β1 demonstrated that TINAGL1 colocalized with integrin α5β1 on the plasma membrane of AGS cells (Fig. 5E). Next, we screened chemokines in the gastric mucosa 14 weeks p.i. in WT and *Tinagl1*$^{-/-}$ mice and found that the expression of only *Ccl2* was decreased and that of *Ccl21* was increased in *Tinagl1*$^{-/-}$ mice (Fig. 5F; Supplementary Fig. 9B). More importantly, the results of blockade experiments revealed that TINAGL1 binding to integrin α5β1 was required for the suppression of CCL21 production and promotion of CCL2 production in GECs (Fig. 5G). Taken together, our data suggest that TINAGL1 interacts with integrin α5β1 on GECs to suppress CCL21 production and promote CCL2 production in GECs.

To identify the TINAGL1-mediated downstream signaling activity that regulates CCL2/CCL21 production, we conducted tandem mass tag (TMT)-labeled quantitative phosphoproteomic analysis and liquid chromatography-tandem mass spectrometry (LC–MS/MS) using lysates from untreated and TINAGL1-treated AGS cells. GO term enrichment analysis with two-tailed Fisher's exact test revealed that the phosphorylated proteins in TINAGL1-treated AGS cells were mainly involved in molecular binding, secretion and transport as well as intracellular signaling (Fig. 5H). Further KEGG pathway analysis (Fig. 5I), pathway mapping of signaling cascades (Fig. 5J) and network analysis of signaling cascades (Fig. 5K) in TINAGL1-treated AGS cells revealed that TINAGL1 inhibited the ERK pathway and activated the NF-κB pathway in GECs. More importantly, signal pathway inhibition experiments revealed that TINAGL1 inhibited the ERK pathway to decrease CCL21 production and activated the NF-κB pathway to increase CCL2 production in GECs (Fig. 5L). Taken together, our data suggest that TINAGL1 suppresses CCL21 production and promotes CCL2 production in GECs by directly binding to integrin α5β1 to inhibit the ERK pathway and activate the NF-κB pathway, respectively.

TINAGL1 inhibits moDC infiltration via the CCL21-CCR7 axis, impairing the specific Th1 response to promote *H. pylori* colonization

To evaluate the potential immunoregulatory role of TINAGL1 in *H. pylori* infection, we first compared the properties of gastric Ly6C^{high} monocytes and moDCs from *H. pylori*-infected WT mice (14 weeks p.i.). RNA sequencing (RNA-seq) and GO analyses indicated that Ly6C^{high} monocytes showed amplified inflammatory properties, whereas moDCs exhibited stronger signatures of antigen presentation and T-cell regulation (Fig. 6A, B). As T cells play key roles in controlling *H. pylori* infection [29], the properties of T-cell regulation by moDCs may be observed following chemotaxis of moDCs regulated by TINAGL1 during *H. pylori* infection. We next found increased CCL21 production in the gastric mucosa of *Tinagl1*$^{-/-}$ mice and decreased CCL21 production in the mice injected with TINAGL1 14 weeks p.i. (Fig. 6C). Again, these results were confirmed by our in vivo BM chimera experiments, in which non-BM-derived TINAGL1-expressing cells were largely responsible for inhibiting CCL21 production in the gastric mucosa during *H. pylori* infection (Fig. 6C). Importantly, gastric CCL21 production was significantly increased in *Tinagl1*$^{\Delta GEC}$ mice compared to their *Tinagl1*$^{flox/flox}$ littermates (Fig. 6C). Taken together, our data demonstrate that TINAGL1 plays an essential role in inhibiting CCL21 production in the gastric mucosa during *H. pylori* infection.

Next, we demonstrated that CCL21 production in mouse primary GECs was negatively regulated in a TINAGL1-dependent manner (Supplementary Fig. 10A) and that gastric moDCs from *H. pylori*-infected mice expressed CCR7, the chemokine receptor for CCL21 (Supplementary Fig. 10D). To further evaluate the contribution of the TINAGL1-CCL21-CCR7 axis to moDC migration in vitro, moDC chemotaxis assays were performed. It was demonstrated that treatment with culture supernatant from *ΔcagA H. pylori*-infected primary GECs of WT mice or from WT *H. pylori*-infected primary GECs of *Tinagl1*$^{-/-}$ mice induced significantly more moDC migration than treatment with culture supernatant from WT *H. pylori*-infected primary GECs of WT mice, and this effect was abolished upon pretreatment with neutralizing Abs against CCL21 and/or CCR7 (Fig. 6D). Finally, we conducted a series of loss- and gain-of-function experiments involving CCL21 in vivo and evaluated moDC accumulation in the gastric mucosa 14 weeks p.i. CCL21 administration significantly increased but neutralization of CCL21 significantly reduced moDC accumulation in the gastric mucosa (Fig. 6E). Collectively, these results suggest that the TINAGL1-CCL21-CCR7 axis contributes to moDC accumulation within the gastric mucosa during *H. pylori* infection.

Th cells and their effector molecules play key roles in *H. pylori* infection [29]. First, the production of the Th1 cell effector molecule IFN-γ but not that of the Th17 cell effector molecule IL-17A or the Th22 cell effector molecule IL-22 in the gastric mucosa was increased in *Tinagl1*$^{-/-}$ mice and decreased in mice injected with TINAGL1 14 weeks p.i. (Fig. 6F; Supplementary Fig. 10B). Again, these results were confirmed by our in vivo BM chimera experiments, in which non-BM-derived TINAGL1-expressing cells were largely responsible for IFN-γ inhibition in the gastric mucosa during *H. pylori* infection (Fig. 6F). Importantly, gastric IFN-γ production was significantly increased in *Tinagl1*$^{\Delta GEC}$ mice compared to that in their *Tinagl1*$^{flox/flox}$ littermates (Fig. 6F). Next, the results of moDC/T-cell coculture experiments showed that gastric moDCs from *H. pylori*-infected mice induced proliferation and IFN-γ production in more Th1 cells from the splenic CD4+ T-cell population in *H. pylori*-infected mice than in the same population from the uninfected counterpart mice (Fig. 6G), suggesting a promoting effect of moDCs on the Th1 response during *H. pylori* infection.

To determine the potential contributions of TINAGL1-mediated inhibition of specific Th1 cell subsets to *H. pylori* colonization, we conducted a series of in vivo adoptive transfer experiments and evaluated bacterial colonization in the gastric mucosa 14 weeks p.i. First, transferring CD4$^+$ T cells from *H. pylori*-infected WT donors into WT recipients effectively reduced *H. pylori* colonization compared to that in WT recipients receiving CD4$^+$ T cells from uninfected WT donors, suggesting that specific CD4$^+$ T cells contributed to the reduction in bacterial colonization (Fig. 6H). Next, transferring CD4$^+$ T cells from *H. pylori*-infected WT donors into *Tinagl1*$^{-/-}$ recipients effectively reduced *H. pylori* colonization compared to that in WT recipients receiving the same CD4$^+$ T cells, suggesting that TINAGL1-mediated inhibition of *H. pylori*-

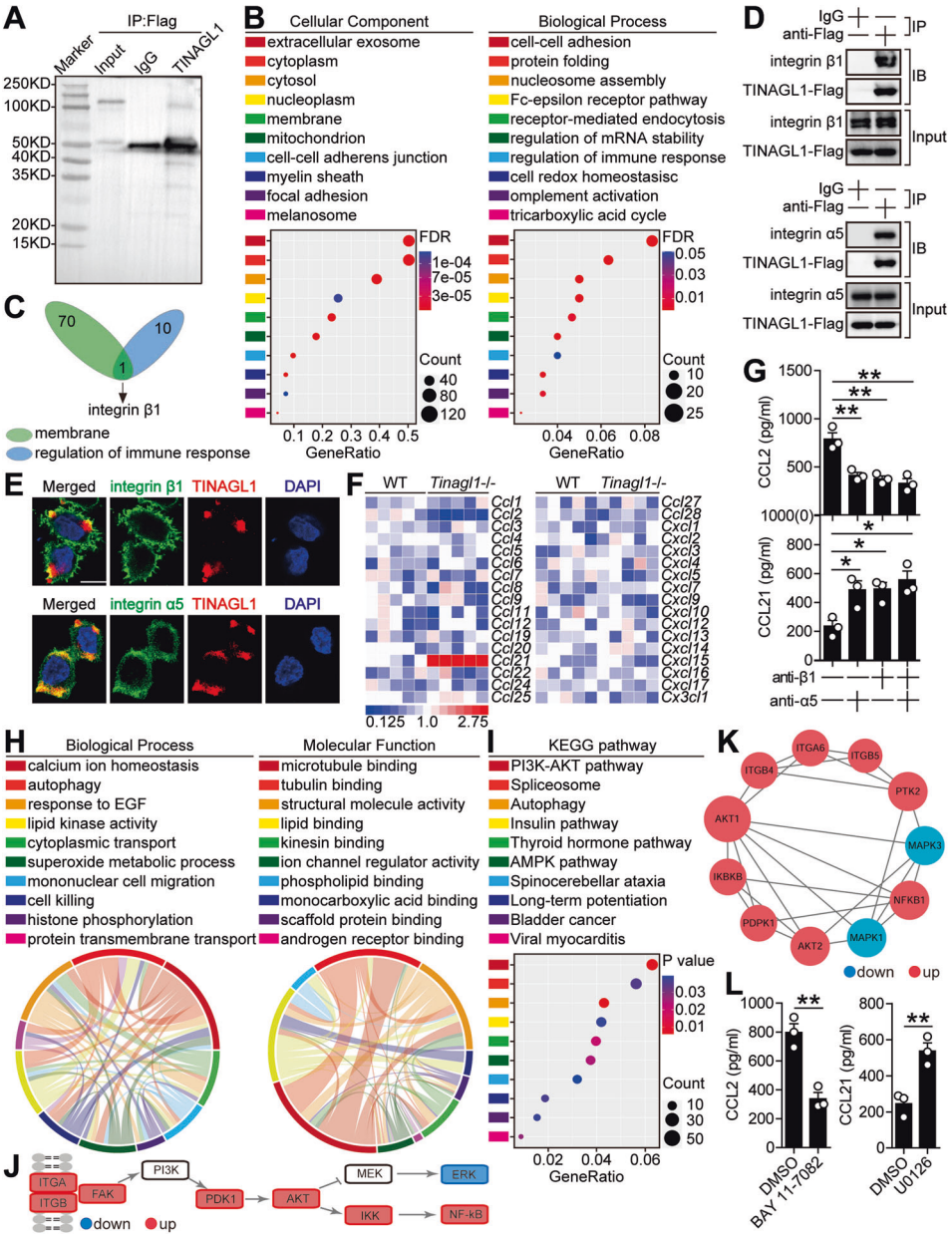

Fig. 5 TINAGL1 suppresses CCL21 production and promotes CCL2 production in GECs by directly binding to integrin α5β1 to inhibit ERK and activate NF-κB, respectively. **A** AGS cells expressing Flag-tagged TINAGL1 (TINAGL1-Flag) were lysed and immunoprecipitated (IP) with IgG (control) or an anti-Flag Ab. The IP samples were subjected to western blotting before mass spectrometry analysis. **B** TINAGL1 interacting partners were clustered by Gene Ontology (GO) analysis, and the top ten GO terms in the "Cellular Component" and "Biological Process" categories are shown. **C** Overlapping genes between the GO term "membrane" in the "Cellular Component" category and the GO term "regulation of immune response" in the "Biological Process" category were identified. Integrin β1 is the core member of each GO term. **D** AGS cells expressing TINAGL1-Flag were lysed and IP with IgG or an anti-Flag Ab. The IP samples were subjected to western blot analysis with the indicated Abs to detect protein interactions with integrin β1 and integrin α5. **E** Confocal microscopy of AGS cells treated with TINAGL1 (100 ng/ml) at 4 °C for 3 h, fixed and stained with anti-TINAGL1, anti-integrin β1 and anti-integrin α5 Abs. **F** The expression of chemokine family members in the gastric mucosa of *H. pylori*-infected WT and *Tinagl1*$^{-/-}$ mice 14 weeks p.i. was analyzed by real-time PCR ($n = 5$). **G** AGS cells were pretreated with anti-integrin β1 and/or anti-integrin α5 neutralizing Abs and then stimulated with TINAGL1 (100 ng/ml) for 24 h. CCL2 and CCL21 production were quantified in cell culture supernatants by ELISA ($n = 3$). **H** AGS cells were treated with TINAGL1 (100 ng/ml) at 37 °C for 3 h, and TINAGL1-activating partners were clustered by GO analysis. The interactions between GO terms in the "Biological Process" and "Molecular Function" categories are shown on a chord diagram colored by GO term. The size of the arc represents the total number of differentially expressed phosphoproteins (DEPPs), and the size of the flow represents the number of DEPPs between the two GO terms. **I** TINAGL1-activating partners were clustered by KEGG pathway analysis, and the top ten pathways are shown. **J** The pathway of PI3K-AKT signaling cascades in TINAGL1-treated AGS cells. **K** The network of PI3K-AKT signaling cascades in (**J**). The circle sizes are proportional to the number of interacting partners. **L** AGS cells were pretreated with U0126 or BAY 11-7082 and then stimulated with TINAGL1 (100 ng/ml) for 24 h. CCL2 and CCL21 production were quantified in cell culture supernatants by ELISA ($n = 3$). Data are representative of 2 independent experiments. Data are shown as the means ± SEMs and were analyzed by Student's *t* test, the Mann–Whitney *U* test or one-way ANOVA. $^{*}P < 0.05$, $^{**}P < 0.01$, n.s. $P > 0.05$ between the groups connected by horizontal lines

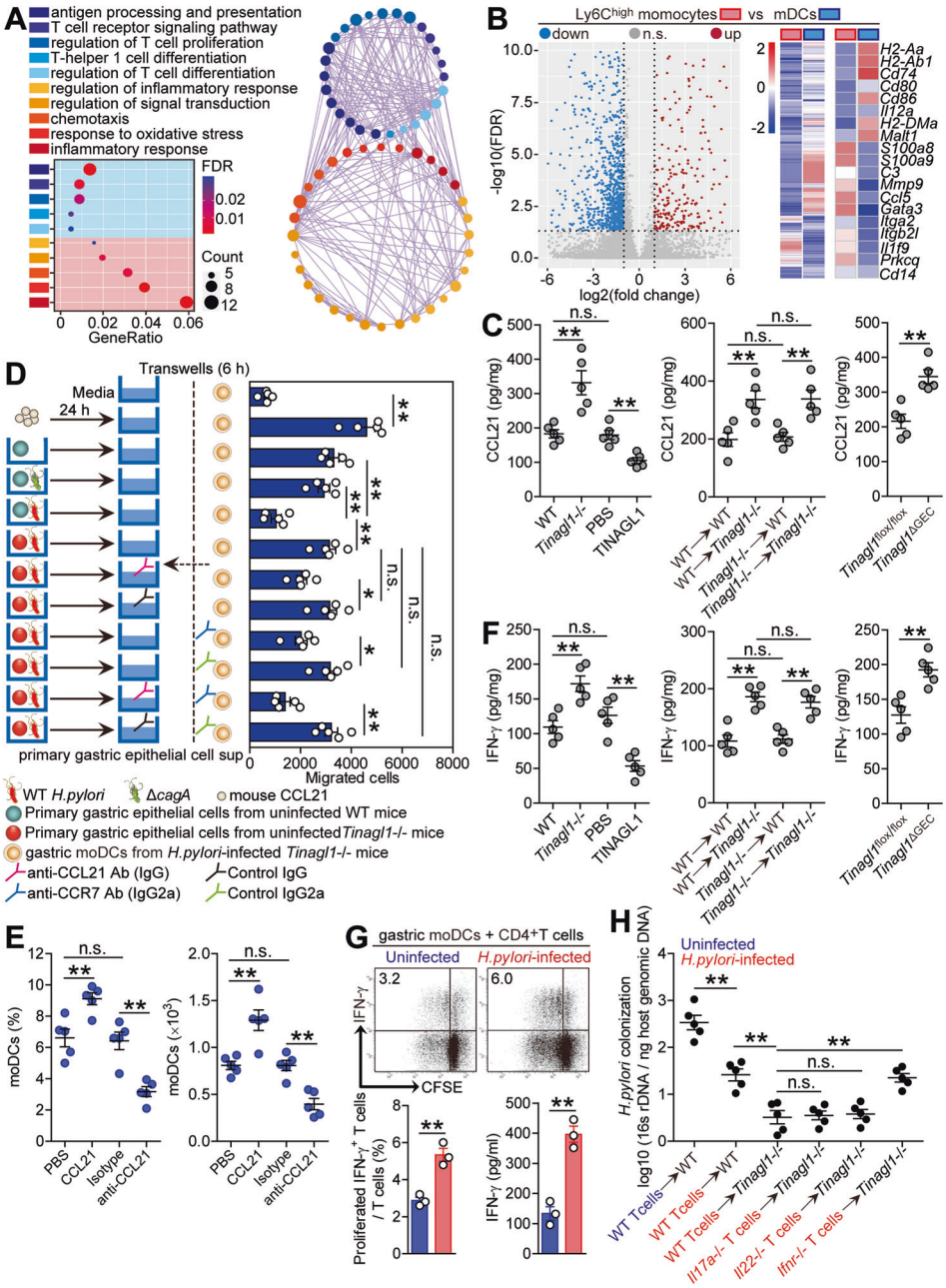

Fig. 6 TINAGL1 inhibits moDC accumulation via the CCL21-CCR7 axis, impairing the specific Th1 cell response to promote *H. pylori* colonization. **A** GO analysis and PPI network analysis of significantly differentially expressed genes in the top five GO terms in Ly6C^{high} monocytes compared with moDCs. **B** Volcano plot and heatmap revealing gene expression changes between Ly6C^{high} monocytes and moDCs. **C** The CCL21 levels in the gastric mucosa of *H. pylori*-infected WT and *Tinagl1*$^{-/-}$ mice, in the gastric mucosa of WT mice injected with TINAGL1 or PBS control, in the gastric mucosa of *H. pylori*-infected BM chimeric mice, and in the gastric mucosa of *H. pylori*-infected *Tinagl1*$^{flox/flox}$ and *Tinagl1*$^{\Delta GEC}$ mice 14 weeks p.i. were compared ($n = 5$). **D** Mouse moDC migration was assessed by transwell assays as described in the Methods section, and the data were statistically analyzed ($n = 5$). **E** The moDC populations in the gastric mucosa of *H. pylori*-infected mice injected with CCL21 or PBS control or with an anti-CCL21 Ab or control IgG 14 weeks p.i. were compared ($n = 5$). The results are expressed as the percentage of moDCs among CD45^{+} cells or the number of moDCs per million total cells in the gastric mucosa. **F** The IFN-γ levels in the gastric mucosa of *H. pylori*-infected WT and *Tinagl1*$^{-/-}$ mice, in the gastric mucosa of WT mice injected with TINAGL1 or PBS control, in the gastric mucosa of *H. pylori*-infected BM chimeric mice, and in the gastric mucosa of *H. pylori*-infected *Tinagl1*$^{flox/flox}$ and *Tinagl1*$^{\Delta GEC}$ mice 14 weeks p.i. were compared ($n = 5$). **G** CFSE-labeled splenic CD4^{+} T cells from uninfected and *H. pylori*-infected mice (14 weeks p.i.) were cocultured for 5 days with FACS-sorted gastric moDCs from *H. pylori*-infected mice (14 weeks p.i.). Representative data and statistical analysis of CD4^{+}IFN-γ^{+} T-cell populations and IFN-γ production are shown ($n = 3$). **H** Bacterial colonization in the gastric mucosa of *H. pylori*-infected WT and *Tinagl1*$^{-/-}$ mice adoptively transferred with splenic CD4^{+} T cells from uninfected or *H. pylori*-infected WT, *Il17a*$^{-/-}$, *Il22*$^{-/-}$ or *Ifnr*$^{-/-}$ mice (14 weeks p.i.) was compared 14 weeks p.i. (n = 5). Data are representative of two independent experiments. Data are shown as the means ± SEMs and were analyzed by Student's *t* test, the Mann–Whitney *U* test or one-way ANOVA. *$P < 0.05$, **$P < 0.01$, n.s. $P > 0.05$ between the groups connected by horizontal lines. sup supernatant

specific CD4$^+$ T cells leads to increased bacterial colonization (Fig. 6H). Finally, transferring CD4$^+$ T cells from *H. pylori*-infected WT donors into *Tinagl1*$^{-/-}$ ecipients effectively reduced *H. pylori* colonization compared to that in *Tinagl1*$^{-/-}$ recipients receiving CD4$^+$ T cells from *H. pylori*-infected *Ifnr*$^{-/-}$ donors but not in *Tinagl1*$^{-/-}$ recipients receiving CD4$^+$ T cells from *Il17a*$^{-/-}$ donors or *Il22*$^{-/-}$ donors, suggesting that TINAGL1 mediates the inhibition of IFN-γ production in *H. pylori*-specific CD4$^+$ T cells (Th1 cells), leading to increased bacterial colonization (Fig. 6H). Overall, these results indicate that TINAGL1 promotes gastric *H. pylori* colonization by inhibiting IFN-γ production by *H. pylori*-specific Th1 cells.

TINAGL1 promotes Ly6C^{high} monocyte accumulation via the CCL2-CCR2 axis and induces S100A11 production by Ly6C^{high} monocytes, contributing to *H. pylori*-associated gastritis

Chemotaxis plays important roles in monocyte migration [30]. We next found that the CCL2 level in the gastric mucosa was decreased in *Tinagl1*$^{-/-}$ mice and increased in mice injected with TINAGL1 14 weeks p.i. (Fig. 7A). Again, these results were confirmed by our in vivo BM chimera experiments, in which non-BM-derived TINAGL1-expressing cells were largely responsible for CCL2 production in the gastric mucosa during *H. pylori* infection (Fig. 7A). Importantly, the gastric CCL2 level was significantly decreased in *Tinagl1*$^{\Delta GEC}$ mice compared to their *Tinagl1*$^{flox/flox}$ littermates (Fig. 7A). Taken together, our data demonstrate that TINAGL1 plays an essential role in promoting CCL2 production in the gastric mucosa during *H. pylori* infection.

Next, we conducted a series of loss- and gain-of-function experiments involving CCL2 in vivo and evaluated Ly6C^{high} monocyte accumulation in the gastric mucosa 14 weeks p.i. CCL2 administration significantly increased but neutralization of CCL2 significantly reduced Ly6C^{high} monocyte accumulation in the gastric mucosa (Fig. 7B). Furthermore, CCL2 production by primary GECs from *H. pylori*-infected mice was positively regulated in a TINAGL1-dependent manner (Fig. 7C; Supplementary Fig. 10G), and gastric Ly6C^{high} monocytes from *H. pylori*-infected mice expressed CCR2, the chemokine receptor for CCL2, in a TINAGL1-independent manner (Supplementary Fig. 10F, H). To further evaluate the contribution of the TINAGL1-CCL2-CCR2 axis to Ly6C^{high} monocyte migration in vitro, Ly6C^{high} monocyte chemotaxis assays were performed. It was demonstrated that treatment with culture supernatant from WT *H. pylori*-infected primary GECs of WT mice induced significantly more Ly6C^{high} monocyte migration than treatment with culture supernatant from WT *H. pylori*-infected primary GECs of *Tinagl1*$^{-/-}$ mice or from *ΔcagA H. pylori*-infected primary GECs of WT mice, and this effect was abolished upon pretreatment with neutralizing Abs against CCL2 and/or CCR2 (Fig. 7D). Collectively, these results suggest that the TINAGL1-CCL2-CCR2 axis contributes to Ly6C^{high} monocyte accumulation within the gastric mucosa during *H. pylori* infection.

To evaluate the effects of TINAGL1 on the infiltrated Ly6C^{high} monocytes during *H. pylori* infection, we stimulated FACS-sorted gastric Ly6C^{high} monocytes from *H. pylori*-infected mice (14 weeks p.i.) with TINAGL1 and performed RNA-seq and GO analyses, identifying the top ten GO terms in the "Cellular Component" and "Molecular Function" categories significantly enriched in the candidate activating partners (Supplementary Fig. 10I), with one candidate, S100A11, overlapping and present in both the GO term "extracellular vesicular exosome" in the "Cellular Component" category and the GO terms "Ca-dependent protein binding" and "S100 protein binding" in the "Molecular Function" category (Fig. 7E). Next, we isolated gastric Ly6C^{high} monocytes and stimulated them with TINAGL1, which led to S100A11 production by these cells in vitro (Fig. 7F, G). We next found that S100A11 was decreased in *Tinagl1*$^{-/-}$ mice and increased in mice injected with TINAGL1 14 weeks p.i. (Fig. 7H). Furthermore, injection of S100A11 significantly increased gastric inflammation but neutralizing S100A11 significantly reduced inflammation in the gastric mucosa 14 weeks p.i. (Fig. 7I). Collectively, our data demonstrate that TINAGL1 plays an essential role in inducing Ly6C^{high} monocyte accumulation and S100A11 production in the gastric mucosa, contributing to *H. pylori*-associated gastritis.

DISCUSSION

During infection, stromal cells can produce various ECM proteins to promote infection-associated pathology [31, 32]. However, relatively little is known regarding ECM proteins that play both procolonization and proinflammatory functional roles. Our study establishes the ECM protein TINAGL1 as a novel matricellular protein that promotes bacterial persistence and gastritis progression in the setting of *H. pylori* infection. To our knowledge, this is the first demonstration of statistically significant correlations between the prevalent high TINAGL1 expression in human gastric samples and persistent infection and/or chronic inflammation; it is also the first demonstration of the role of infection-induced TINAGL1 as a matricellular protein in the regulation of inflammatory immune responses within the gastric environment.

In this study, we not only identified a previously unrecognized role for TINAGL1 during *H. pylori* infection but also showed that TINAGL1 expression is readily induced in primary gastric tissues and GECs upon ex vivo infection. This response is consistent with our previous observations on TINAGL1 expression in tumor cells [33]. Several ECM proteins, such as fibronectin [34], are known to be induced by inflammatory cytokines, such as TGF-β [35] and TNF-α [36]. In our case, we identified a new cytokine regulating TINAGL1 expression during *H. pylori* infection, IL-1β: IL-1β exerts a synergistic effect on TINAGL1 induction by activating the ERK-SP1 pathway. These findings, together with previous observations on the pathologic effects of IL-1β during *H. pylori* infection [37, 38], point to the combined activities of IL-1β and *H. pylori* as important determinants of TINAGL1 induction in the gastric mucosa.

Evidence in cancers supports the idea that TINAGL1 mediates many of the environmental changes that lead to either protection or pathology: TINAGL1 plays protective roles in TNBC [12]; however, it contributes to HCC progression [13]. TINAGL1 may also contribute pathologically in the *H. pylori*-infected gastric environment, where TINAGL1 is produced by GECs and high TINAGL1 expression is found in clinical samples in association with disease development. Given the apparent relationship between TINAGL1 levels and the severity of gastric inflammation in *H. pylori*-infected human patients observed in this study, TINAGL1 should be considered as a novel diagnostic biomarker for *H. pylori*-associated diseases.

The pathologic roles of ECM proteins have been suggested to involve various mechanisms [39, 40]. Integrins are key cell surface receptors that connect intracellular structures to ECM components, including matricellular proteins, and perform important signaling functions [41, 42]. Tumor cell-expressed integrins, including integrin α5β1, have been reported to interact with TINAGL1 to regulate cancer progression [12], consistent with our findings indicating that the integrin signaling pathway is regulated by TINAGL1. In line with these findings, we identified that TINAGL1 suppresses CCL21 production and promotes CCL2 production in GECs by directly binding to integrin α5β1 to inhibit the ERK pathway and activate the NF-κB pathway, respectively. More importantly, we further demonstrated, for the first time, that TINAGL1 suppresses CCL21 production in GECs, leading to increased bacterial colonization due to an impaired *H. pylori*-specific host Th1 response. IFN-γ, one of the key effector molecules of Th1 cells, is reported to play key roles in controlling *H. pylori* infection in mice [43] and humans [44]. For instance, IFN-γ deficiency results in uncontrolled colonization of *H. pylori* in the gastric mucosa [45]. Notably, our findings mechanistically connect the pathological roles of TINAGL1 with an impaired *H. pylori*-

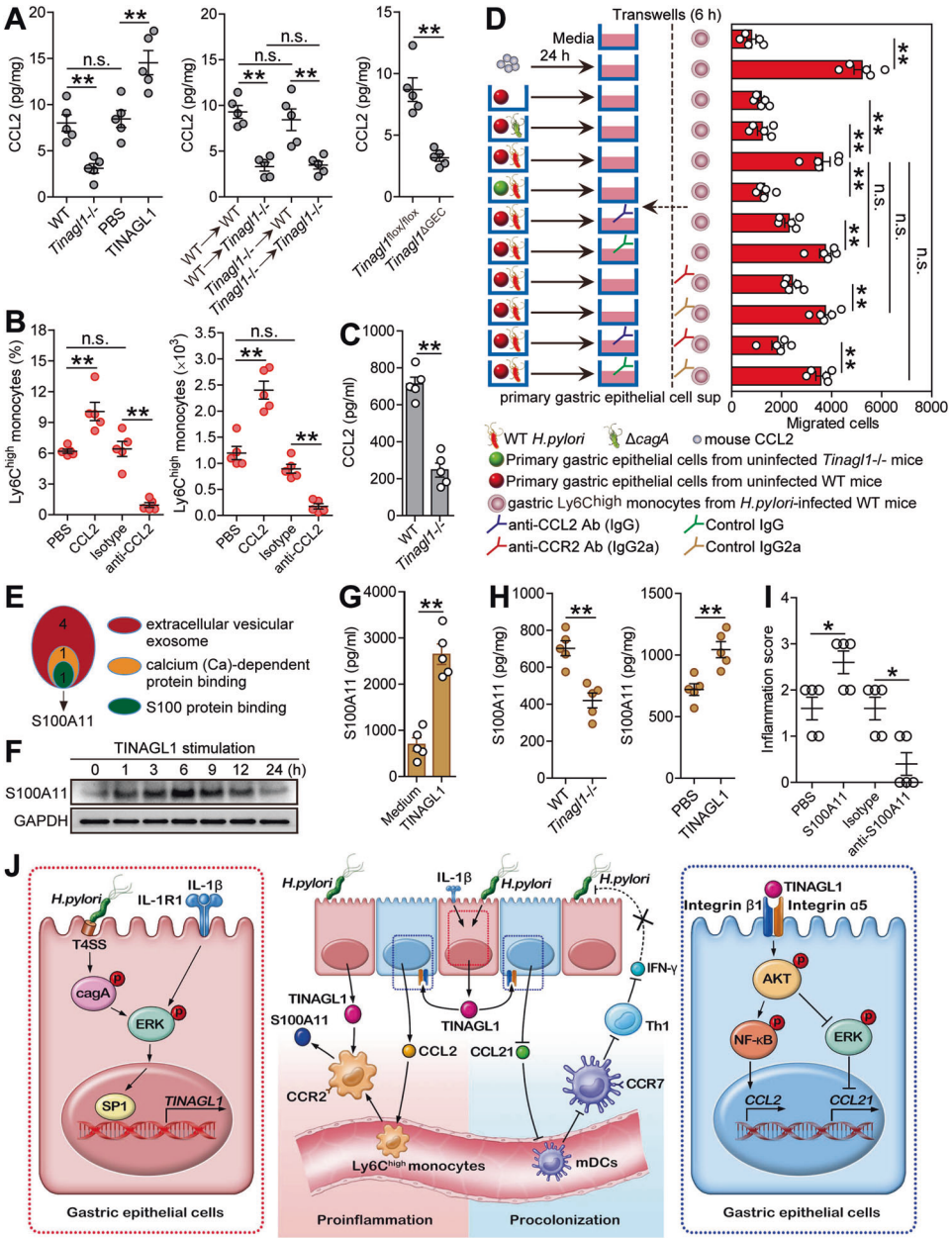

Fig. 7 TINAGL1 promotes Ly6C^{high} monocyte accumulation via the CCL2-CCR2 axis and induces S100A11 production by Ly6C^{high} monocytes, contributing to *H. pylori*-associated gastritis. **A** The CCL2 levels in the gastric mucosa of *H. pylori*-infected WT and *Tinagl1*$^{-/-}$ mice, in the gastric mucosa of WT mice injected with TINAGL1 or PBS control, in the gastric mucosa of *H. pylori*-infected BM chimeric mice, and in the gastric mucosa of *H. pylori*-infected *Tinagl1*$^{flox/flox}$ and *Tinagl1*$^{\Delta GEC}$ mice 14 weeks p.i. were compared ($n = 5$). **B** The Ly6C^{high} monocyte populations in the gastric mucosa of *H. pylori*-infected mice injected with CCL2 or PBS control or with an anti-CCL2 Ab or control IgG 14 weeks p.i. were compared ($n = 5$). The results are expressed as the percentage of Ly6C^{high} monocytes among CD45^{+} cells or the number of Ly6C^{high} monocytes per million total cells in the gastric mucosa. **C** Primary GECs from uninfected WT and *Tinagl1*$^{-/-}$ mice were infected with WT *H. pylori* (MOI = 100) for 24 h. CCL2 production was quantified in cell culture supernatants by ELISA ($n = 5$). **D** Mouse Ly6C^{high} monocyte migration was assessed by transwell assays as described in the Methods section, and the data were statistically analyzed ($n = 5$). **E** FACS-sorted gastric Ly6C^{high} monocytes from *H. pylori*-infected mice (14 weeks p.i.) were stimulated with TINAGL1 (100 ng/ml) for 3 h. Overlapping genes between the GO term "extracellular vesicular exosome" in the "Cellular Component" category and the GO terms "Ca-dependent protein binding" and "S100 protein binding" in the "Molecular Function" category were identified. S100A11 is the core member of each GO term. S100A11 protein expression in FACS-sorted gastric Ly6C^{high} monocytes from *H. pylori*-infected mice (14 weeks p.i.) stimulated with TINAGL1 for different time points (**F**) or 24 h (**G**) was analyzed. **H** The S100A11 levels in the gastric mucosa of *H. pylori*-infected WT and *Tinagl1*$^{-/-}$ mice and in the gastric mucosa of WT mice injected with TINAGL1 or PBS control 14 weeks p.i. were compared ($n = 5$). **I** Histological scores of inflammation in the gastric mucosa of *H. pylori*-infected mice injected with S100A11 or PBS control or with an anti-S100A11 Ab or control IgG 14 weeks p.i. were compared ($n = 5$). **J** A proposed model of crosstalk among *H. pylori*, IL-1β, GECs, TINAGL1, Ly6C^{high} monocytes and moDCs leading to TINAGL1-mediated procolonization and proinflammatory effects in the gastric mucosa during *H. pylori* infection. Data are representative of two independent experiments. Data are shown as the means ± SEMs and were analyzed by Student's *t* test, the Mann–Whitney *U* test or one-way ANOVA. $^{*}P < 0.05$, $^{**}P < 0.01$, n.s. $P > 0.05$ between the groups connected by horizontal lines. sup supernatant

specific host Th1 response. Regarding the regulation of inflammation, we demonstrated that TINAGL1 promotes CCL2 production in GECs, which results in increased gastric influx of Ly6C^{high} monocytes via CCL2-CCR2-dependent migration. Consistent with the inflammatory potential of Ly6C^{high} monocytes in *C. albicans* infection [46], we further demonstrated that TINAGL1 induces the production of the proinflammatory protein S100A11 in Ly6C^{high} monocytes, thereby promoting *H. pylori*-associated gastritis.

Our results from both the in vitro and in vivo gain- and loss-of-function experiments identified the matricellular protein TINAGL1 as a novel pathological regulator that promotes *H. pylori* colonization and contributes to gastritis and support the concept that TINAGL1 acts through a two-pronged mechanism involving both suppression of the host adaptive defense and promotion of inflammatory responses. Specifically, our data collectively identify a multistep model of chronic gastritis accompanied by persistent *H. pylori* infection that involves interactions among *H. pylori*, IL-1β, GECs, TINAGL1, Ly6C^{high} monocytes and moDCs within the gastric mucosa (Fig. 7J). In conclusion, we reveal the functional role of the regulatory network with TINAGL1 as the core in *H. pylori*-associated gastritis. These findings will likely contribute to the development of precise treatment strategies to alleviate *H. pylori*-associated gastritis. Although we found in this study that α5β1 is the only receptor for TINAGL1, we believe that TINAGL1, as the core of the regulatory network and an ECM protein, is the more feasible and more desirable target, especially in view of the wide range of integrin expression. We envisage that strategies including agents such as monoclonal antibodies, small molecule inhibitors and traditional Chinese medicine components, could all be further pursued. Indeed, we identified several preliminary components and are currently evaluating their applications in preclinical in vivo studies. In the future, it will be interesting to determine whether targeting the TINAGL1-associated molecular pathways and cellular networks described here in the context of *H. pylori* infection can improve the outcome of the associated diseases caused by this pathogen.

MATERIALS AND METHODS

Patients and specimens

Gastric biopsy specimens and blood were collected from 81 *H. pylori*-infected and 36 uninfected patients who underwent upper esophagogastroduodenoscopy for dyspeptic symptoms at XinQiao Hospital (Supplementary Table 1). *H. pylori* infection was diagnosed by the [^{14}C] urea breath test and rapid urease test of antral biopsy specimens and subsequently confirmed by real-time PCR for 16S rDNA and serological testing for *H. pylori*-specific antibodies (Abs). For isolation of human primary gastric epithelial cells (GECs), fresh nontumor gastric tissues (obtained from a region at least 5 cm from the tumor site) were obtained from gastric cancer patients who underwent surgical resection at Southwest Hospital and were determined to be negative for *H. pylori* infection as described above. None of these patients had received chemotherapy or radiotherapy before sampling. Individuals with atrophic gastritis, hypochlorhydria, antibiotic treatment, autoimmune disease, infectious diseases or multiple primary cancers were excluded.

Antibodies and other reagents

See Supplementary Table 2.

Mice

C57BL/6 *Tinagl1*$^{-/-}$ mice were generated by crossing *Tinagl1*$^{flox/flox}$ mice (Cyagen Biosciences, China) with B6.FVB-Tg(EIIa-cre)C5379Lmgd/J (*E2a-Cre*, IMSR_JAX:003724) mice, and wild-type (WT) littermates were used as controls (Supplementary Fig. 4A, B). C57BL/6 *Il1r1*$^{-/-}$ mice (IMSR_JAX:003245) were obtained from The Jackson Laboratory (USA). C57BL/6 *Il17a*$^{-/-}$ mice and C57BL/6 *Ifnr*$^{-/-}$ mice were kindly provided by Dr. Richard A. Flavell (Yale University, USA). C57BL/6 *Il22*$^{-/-}$ mice were obtained from Dr. Wenjun Ouyang (Genentech, USA). *Tinagl1* GEC-specific knockout mice (*Atp4b-Cre;Tinagl1*$^{flox/flox}$, also known as called*Tinagl1*$^{\Delta GEC}$) were generated by crossing *Tinagl1*$^{flox/flox}$ mice with B6.FVB-Tg(Atp4b-cre) 1Jig/JcmiJ (*Atp4b-Cre*, IMSR_JAX:030656) mice, and *Tinagl1*$^{flox/flox}$ littermates were used as controls (Supplementary Fig. 4D). Only female mice were used in all experiments except for the chimera experiments, in which male mice were also used, and were free of Abs specific for pathogenic murine viruses; negative for pathogenic bacteria, including *Helicobacter* spp., and parasites; and were maintained under specific pathogen-free conditions in a barrier sustained facility and provided sterile food and water [19].

Bacterial culture and infection of mice with bacteria

H. pylori NCTC 11637 (*cagA*-positive) (WT *H. pylori*) and *cagA*-knockout *H. pylori* NCTC 11637 (*ΔcagA*) were grown on brain-heart infusion plates containing 10% rabbit blood at 37 °C under microaerophilic conditions. For mouse infection, bacteria were propagated in Brucella broth supplemented with 5% fetal bovine serum (FBS) at 37 °C with gentle shaking under microaerobic conditions. After culture for 1 d, live bacteria were collected, and the concentration was adjusted to 10^9 CFU/ml. Mice were fasted overnight and orogastrically inoculated with bacteria (3×10^8 CFU) on two occasions at 1 d intervals. The *H. pylori* infection status and *H. pylori*-induced gastritis in murine experiments were confirmed using real-time PCR for *H. pylori* 16S rDNA, the urease biopsy test, Warthin-Starry staining and immunohistochemical staining for *H. pylori*, and evaluation of inflammation by hematoxylin and eosin (H&E) staining.

Generation of bone marrow chimeric (BM) mice

The following BM chimeric mice were generated: male WT BM→female WT mice, male WT BM→female *Tinagl1*$^{-/-}$ mice, male *Tinagl1*$^{-/-}$ BM→female WT mice, and male *Tinagl1*$^{-/-}$ BM→female *Tinagl1*$^{-/-}$ mice. BM cells were collected from the femurs and tibias of donor mice by aspiration and flushing and were suspended in PBS at a concentration of 5×10^7 cells/ml. The BM in recipient mice was ablated with lethal irradiation (8 Gy). Then, the recipient mice were anesthetized and inoculated intravenously with 1.5×10^7 BM cells from the donor mice in a volume of 300 μl of sterile PBS. Then, the transplanted BM was allowed to regenerate for 8 weeks before subsequent experimental procedures were performed. To verify successful engraftment and reconstitution of the BM in the host mice, genomic DNA was isolated from tail tissues of each chimeric mouse 8 weeks after BM transplantation. Quantitative PCR was performed to detect the *Sry* gene on the Y chromosome (primers are listed in Supplementary Table 3) and the mouse *β2-microglobulin* gene as an internal control. The rates of chimera generation were calculated with the assumption that the ratio of *Sry* gene expression to *β2-microglobulin* gene expression was 100% in female recipient mice. We confirmed that the rates of chimera generation were consistently higher than 90%. After BM reconstitution was confirmed, mice were infected with bacteria as described above.

TINAGL1/chemokine/antibody administration

One day after infection with WT *H. pylori* as described above, WT mice were injected intraperitoneally with 25 μg of recombinant mouse TINAGL1, recombinant mouse CCL2, recombinant mouse CCL21, or recombinant mouse S100A11 or with anti-mouse CCL21, anti-mouse CCL21, or anti-mouse S100A11 Abs or control IgG (100 μg), and injections were repeated every week until the mice were sacrificed.

T-cell adoptive transfer

The donor mice (WT mice, *Il17a*$^{-/-}$ mice, *Il22*$^{-/-}$ mice or *Ifnr*$^{-/-}$ mice) were orogastrically inoculated with *H. pylori* as described above, and infection was allowed to progress for 14 weeks. Then, the donor mice were sacrificed for purification of splenic CD4$^+$ T cells. One day before infection with *H. pylori*, the recipient mice (WT mice or *Tinagl1*$^{-/-}$ mice) were injected intravenously (1×10^6 cells/mouse) with purified splenic CD4$^+$ T cells (StemCell Technologies) from uninfected WT mice or *H. pylori*-infected WT mice, *Il17a*$^{-/-}$ mice, *Il22*$^{-/-}$ mice or *Ifnr*$^{-/-}$ mice (14 weeks p.i.). The recipient mice were then infected with bacteria as described above and sacrificed 14 weeks p.i. for bacterial colonization evaluation.

Evaluation of bacterial colonization

Mice were sacrificed at the indicated times. An incision was made in the greater curvature of the stomach, and one half of the stomach tissue was cut into four parts for RNA extraction, DNA extraction, protein extraction, and tissue fixation for immunohistochemical staining. DNA from biopsy specimens was extracted with a QIAamp DNA Mini Kit. As previously

described [47], *H. pylori* colonization was quantified by analysis of *H. pylori*-specific 16S rDNA using specific primers and probes (Supplementary Table 3) by the TaqMan method. The amount of mouse β2-microglobulin DNA in the same specimen was used to normalize the values. Based on a previous study [48], the density of *H. pylori* was shown as the number of bacterial genomes per nanogram of host genomic DNA [18]. The other half of the stomach tissue was used for isolation of single cells as described below. The isolated single cells were collected and analyzed by flow cytometry.

Evaluation of inflammation

Mice were sacrificed at the indicated times. An incision was made in the greater curvature of the stomach for H&E staining. The degree of inflammation was evaluated independently by two pathologists according to previously established criteria [19, 49].

Isolation of single cells from tissues

Fresh tissues were washed three times with Hank's solution containing 1% FBS, cut into small pieces, collected in RPMI 1640 medium containing 1 mg/ml collagenase IV and 10 mg/ml DNase I, and then mechanically dissociated by using a gentleMACS Dissociator (Miltenyi Biotec). The dissociated cells were further incubated for 0.5−1 h at 37 °C under continuous rotation. The cell suspensions were then filtered through 70-μm cell strainers (BD Labware).

Cell/tissue culture and stimulation

Primary GECs were purified from gastric tissue single-cell suspensions from uninfected human donors or mice with a MACS column purification system using anti-human or anti-mouse CD326 magnetic beads (Miltenyi Biotec), respectively. The sorted primary GECs were used only when their viability was determined to be >90% and their purity was determined to be >95%. The cells were cultured in complete RPMI 1640 medium supplemented with 10% FBS in a humidified environment containing 5% CO_2 at 37 °C. Human GEC lines (AGS cells, GES-1 cells, HGC-27 cells) were obtained from the American Type Culture Collection (ATCC, Manassas, VA, USA). Human GEC lines, primary GECs and primary gastric mucosa tissues from uninfected human donors or mice were infected with WT *H. pylori* or *ΔcagA H. pylori* at a multiplicity of infection (MOI) of 100 for 24 h. AGS cells and primary GECs were also infected with WT *H. pylori* (MOI = 100) in the presence or absence of IL-1β (100 ng/ml) for 24 h. AGS cells and primary GECs were also infected with WT *H. pylori* at different MOIs (for 24 h), at the indicated time points (MOI = 100), or in the presence or absence of IFN-γ, IL-4, IL-17A, IL-22, IL-12, IL-6 or IL-23 (100 ng/ml) for 24 h (MOI = 100). For IL-1β or signaling pathway inhibition experiments, AGS cells were pretreated with a neutralizing Ab against IL-1β (20 μg/ml) or control IgG (20 μg/ml) or with U0126, PP2, SB203580, SP600125, Wortmannin, AG490, BAY 11-7082 (20 μM) or dimethyl sulfoxide (DMSO) for 2 h. For IL-1R1 inhibition experiments, AGS cells were pretreated with *IL1R1* siRNA or nonspecific control siRNA (NC) (40 nM) for 24 h. For transwell assays, AGS cells were added to the lower chamber of the transwell plate, WT *H. pylori* cells (MOI = 100) were placed into the lower or upper chamber of the transwell plate (0.4-μm pore size), and the transwell plates were then incubated for 24 h. After coculture, cells were collected for real-time PCR and western blot analyses, and the culture supernatants were harvested for ELISA.

Chemotaxis assay

Mouse gastric Ly6C^{high} monocytes and moDCs from *H. pylori*-infected WT mice (14 weeks p.i.) were sorted by a fluorescence-activated cell sorter (FACS) (FACSAria III; BD Biosciences). Mouse primary GECs were purified from gastric tissue single-cell suspensions from uninfected mice with a MACS column purification system using anti-mouse CD326 magnetic beads (Miltenyi Biotec) and then stimulated with WT *H. pylori* or *ΔcagA H. pylori* (MOI = 100) for 24 h. The culture supernatants were collected and used as a source of chemoattractants in the chemotaxis assay. For the chemotaxis assay, sorted cells (1×10^5) were transferred into the upper chambers of transwell plates (5-μm pore size). CCL2/CCL21 (100 ng/ml) and culture supernatants from various cultures were placed in the lower chambers. After 6 h of culture, migration was quantified by counting the cells in the lower chamber and the cells adhering to the bottom surface of the membrane. In some cases, blocking Abs specific for mouse CCL2/CCL21 (20 μg/ml) or control IgG (20 μg/ml) was added to the culture supernatants and blocking Abs specific for mouse CCR2/CCR7 (20 μg/ml) or control IgG (20 μg/ml) was added to the cell suspensions and incubated for 2 h before the chemotaxis assay.

In vitro T-cell culture system

Purified splenic CD4$^+$ T cells from uninfected or *H. pylori*-infected WT mice (14 weeks p.i.) were labeled with carboxyfluorescein succinimidyl ester (CFSE) and cocultured (1×10^5 cells/well) with FACS-sorted gastric moDCs from *H. pylori*-infected WT mice (14 weeks p.i.) at a 2:1 ratio in 200 μl of RPMI 1640 medium containing recombinant mouse IL-2 (20 IU/ml), anti-CD3 Abs (2 μg/ml), and anti-CD28 (1 μg/ml) Abs. After a 5-d incubation, the cells were collected and subjected to intracellular cytokine staining, and the culture supernatants were harvested for ELISA.

Luciferase reporter assay

Promoter constructs containing the region containing positions −2000 to 0 in the *TINAGL1* gene were amplified from human genomic DNA by PCR. The amplified full-length sequence or sequence fragments were inserted into the NheI and HindIII sites in the pGL3-basic vector by Sangon Biotech (Shanghai, China). For the luciferase reporter assay, cells were seeded in 24-well plates and transfected at approximately 80% confluence with the constructed luciferase reporter vector for 4 h. Lipofectamine 2000 was used to transfect AGS cells according to the manufacturer's protocols. Luciferase activity was measured to assess promoter activity after WT *H. pylori* (with or without U0126 pretreatment) or Δ*cagA H. pylori* infection (MOI = 100) for 24 h and after WT *H. pylori* infection (MOI = 100) in the presence or absence of IL-1β (100 ng/ml) (with or without pretreatment with U0126 or neutralizing Abs against IL-1β) for 24 h with a dual-luciferase reporter assay system following the manufacturer's protocol. Luciferase activity was normalized to Renilla luciferase activity.

Chromatin Immunoprecipitation (ChIP)

AGS cells were infected with WT *H. pylori* or *ΔcagA H. pylori* (MOI = 100) or stimulated with WT *H. pylori* (MOI = 100) and IL-1β (100 ng/ml) for 24 h. The cells were then treated at room temperature for 10 min with 1% formaldehyde in cell culture medium. Glycine (11% in medium) solution was then gently mixed with the cultures at room temperature for 5 min to terminate crosslinking. The cells were washed twice with ice-cold PBS and centrifuged at 3000 × *g* for 5 min. Membrane extraction buffer containing protease/phosphatase inhibitors was then added to each pelleted sample. The cell lysates were pulse-sonicated on ice; then, the supernatants containing digested chromatin were collected into two tubes as the input and immunoprecipitation samples. Anti-SP1 Abs or control IgG was added, and IP reactions were conducted overnight at 4 °C with agitation. ChIP-grade protein A/G magnetic beads were then added to each IP reaction. Two hours later, the beads were collected and washed, and the bound immunoprecipitates were eluted with 5 M NaCl containing 20 μg/ml Proteinase K. Crosslinking was reversed by heating to 65 °C for 1.5 h, and DNA was purified. Purified DNA samples were analyzed by PCR with designed primers (Supplementary Table 5).

Generation of AGS cells expressing Flag-tagged TINAGL1 (TINAGL1-Flag)

The full-length human TINAGL1 CDS (NCBI Gene ID: 64129), with the Flag tag inserted directly downstream of the start codon, was chemically synthesized and inserted into the pLVX-mCMV-ZsGreen1-Puro lentiviral vector at the EcoRI and BamHI restriction sites. The above reconstructed plasmids were transiently transfected into AGS cells, and immunoprecipitation (IP) and western blotting were applied to confirm TINAGL1 overexpression. Briefly, adherent cells were lysed with precooled IP dilution buffer (20 mM Tris-HCl, 2 mM EDTA, 1% Triton X-100, 150 mM NaCl) supplemented with PMSF and protein inhibitor complex (PIC) on ice. Cellular debris was removed by centrifugation at 12,000 rpm and 4 °C for 10 min, and the supernatant was retained for subsequent IP. In detail, the total cell lysate was divided into two equal parts, which were incubated with a mouse anti-Flag monoclonal Ab or mouse IgG isotype. After gentle agitation at 4 °C overnight, pretreated Pierce™ Protein G Magnetic beads were added to the lysate samples and incubated at 4 °C for 4 h with agitation. Next, the immunoprecipitated protein complexes were enriched using a magnetic separator and collected in elution buffer (10% SDS, 0.5 M EDTA, 1 M Tris-HCl), and protein expression was validated by western blotting.

Mass spectrometry (MS) analysis

Samples were sent to Sangon Biotech (Shanghai, China) for MS analysis. In brief, the samples were subjected to in-gel digestion and then analyzed by online nanospray LC–MS/MS on a Q Exactive™ HF mass spectrometer (Thermo Fisher Scientific, USA) coupled to an EASY-nanoLC 1000 system

(Thermo Fisher Scientific, USA). The peptides (3 µl) were loaded (analytical column: Acclaim PepMap C18, 75 µm × 25 cm) and separated with a 60 min gradient. The column flow rate was maintained at 300 nl/min, with the column temperature controlled at 40 °C. An electrospray voltage of 2 kV across the inlet of the mass spectrometer was used. The mass spectrometer was run in data-dependent acquisition mode and automatically switched between MS and MS/MS acquisition. Tandem mass spectra were processed by PEAKS Studio version X+ (Bioinformatics Solutions Inc., Waterloo, Canada). PEAKS DB was set up to search the uniprot_homo_sapiens_201907 database (ver 201907, 20414 entries) assuming trypsin as the digestion enzyme.

Immunoprecipitation (IP) assay

The immunoprecipitation assay was performed using a Pierce™ Classic Magnetic IP/Co-IP Kit following the manufacturer's protocol. Whole-cell extracts of AGS cells expressing TINAGL1-Flag were lysed with IP lysis/wash buffer containing a protease inhibitor. After centrifugation for 10 min at 13,000 × *g*, the supernatants were collected and incubated with an anti-Flag Ab or control IgG at 4 °C overnight. After overnight incubation, the protein A/G magnetic beads (washed three times with IP Lysis/Wash Buffer) were incubated with the whole-cell lysates for 1 h at room temperature with gentle shaking. Then, the beads were washed three times with IP Lysis/Wash Buffer, resuspended in 50 µl of 1% (w/v) SDS sample buffer and boiled at 97 °C for 10 min. Proteins were separated by SDS–PAGE (10% SDS) and transferred to a PVDF membrane for western blot analysis.

Immunofluorescence

AGS cells were treated with TINAGL1 (100 ng/ml) at 4 °C for 3 h and then fixed. Paraformaldehyde-fixed frozen tissue sections or AGS cells were washed in PBS, blocked for 30 min with 20% goat serum in PBS, and subjected to staining for TINAGL1 and integrin α5, TINAGL1 and integrin β1, or TINAGL1 and H^+/K^+ ATPase β. The slides were examined with a confocal fluorescence microscope (LSM 510 META, Zeiss).

Real-time PCR

DNA from biopsy specimens was extracted with a QIAamp DNA Mini Kit, and RNA of biopsy specimens and cultured cells was extracted with TRIzol reagent. The RNA samples were reverse transcribed into cDNA with the PrimeScript™ RT Reagent Kit. Real-time PCR was performed on an IQ5 system (Bio-Rad) with Real-time PCR Master Mix according to the manufacturer's specifications. The expression levels of 16S rDNA and *cagA*, *TINAGL1/Tinagl1*, *IL1R1*, *IL1B/Il1b*, *Ifnr*, *Il17a*, *Il22*, chemokine and matricellular protein-encoding mRNAs were measured using the TaqMan and/or SYBR Green method with the relevant primers (Supplementary Table 3). For mouse samples, the mouse *β2-microglobulin/β-actin* mRNA level was used for normalization, and its levels in the stomach/cells of uninfected or WT mice were used for calibration. For human samples, the human *GAPDH* mRNA level was used for normalization, and its levels in unstimulated/uninfected/NC-treated cells or the stomachs of uninfected donors were used for calibration. Relative gene expression was expressed as the fold change in the relevant mRNA expression level calculated by the ΔΔCt method.

Flow cytometry

Cell surface markers were stained with specific or isotype control Abs. For analysis of intracellular molecules, cells were stimulated for 5 h with PMA (50 ng/ml) plus ionomycin (1 µg/ml) in the presence of GolgiStop. Intracellular cytokine staining was performed after fixation and permeabilization using Perm/Wash solution. Then, the cells were analyzed by multicolor flow cytometry on a FACSCanto™ instrument (BD Biosciences). Data were analyzed with FlowJo (TreeStar) or FACSDiva (BD Biosciences) software.

ELISA

Isolated human and mouse gastric tissues were homogenized in 1 ml of sterile Protein Extraction Reagent and centrifuged. Tissue/cell supernatants were collected for ELISA. The concentrations of TINAGL1, CCL2, CCL21, IFN-γ and S100A11 in the tissue/cell supernatants were measured using ELISA kits according to the manufacturer's instructions.

Western blot analysis

Protein separation was performed with equal amounts of cell or tissue lysate for each sample on 10−15% SDS–PAGE gels, and proteins were transferred to PVDF membranes. The PVDF membrane were incubated with five percent skim milk for blocking. Mouse TINAGL1 and S100A11 were detected with rabbit anti-TINAGL1 Abs and rabbit anti-S100A11 Abs, respectively; human TINAGL1, ERK1/2, p-ERK1/2, IL-1R1, integrin α5 and integrin β1 were detected with rabbit anti-TINAGL1 Abs, rabbit anti-ERK1/2 Abs, rabbit anti-p-ERK1/2 Abs, mouse anti-IL-1R1 Abs, rabbit anti-integrin α5 Abs and rabbit anti-integrin β1 Abs, respectively. This detection step was followed by incubation with HRP-conjugated secondary Abs. Bound proteins were visualized using a Super ECL plus Western Blotting Kit (Bioground, China).

Tandem mass tag (TMT)-labeled quantitative phosphoproteomic analysis

AGS cells were treated with or without TINAGL1 (100 ng/ml) at 37 °C for 3 h. Following centrifugation, the precipitate was washed with PBS and immediately frozen in liquid nitrogen. Then, the sample was sent to Jingjie PTM BioLab Co., Ltd. (Hangzhou, China) for analysis. Briefly, after thawing, the sample was sonicated three times on ice using a high-intensity ultrasonic processor (Scientz) in lysis buffer containing 8 M urea, 1% phosphatase inhibitor cocktail, and 1% protease inhibitor cocktail. The remaining debris was removed by centrifugation at 12,000 × *g* and 4 °C for 10 min. Finally, the supernatant was collected, and the protein concentrations were determined with a BCA Protein Assay kit according to the manufacturer's instructions. For TMT phosphoproteomic analysis, the same amount of protein from each sample was used. The protein solution was incubated on ice for 2 h and centrifuged (4 °C, 4500 × *g*, 5 min). The precipitate was washed three times with precooled acetone. Tetraethylammonium bromide (TEAB, 200 mM) was added to resuspend the protein pellet, and trypsin was added at a 1:50 trypsin:protein mass ratio for digestion overnight at 37 °C. The digests were incubated at 37 °C for 30 min with DL-dithiothreitol (DTT, 5 mM) and then incubated at room temperature for 15 min in the dark with iodoacetamide (IAM, 11 mM). Using a Strata X C18 SPE column, the tryptic peptides were desalted, vacuum-dried, reconstituted in TEAB (0.5 M) and further labeled with TMTs in accordance with the manufacturer's instructions. The labeled tryptic peptides were fractionated by high-pH reverse-phase HPLC using a BETASIL C18 column (5 µm particles, 4.6 mm, 250 × 10 mm). The peptides were separated into 54 fractions with a gradient of 8–32% acetonitrile over 80 min. Then, the peptides were dried by vacuum centrifugation. The peptide mixtures were first incubated with IMAC microsphere suspensions in loading buffer (50% acetonitrile/0.5% acetic acid) under vibration. To remove the nonspecifically adsorbed peptides, the IMAC microspheres were washed. To elute the enriched phosphopeptides, elution buffer containing 10% NH_4OH was added, and the enriched phosphopeptides were eluted under vibration. The supernatant containing phosphopeptides was collected and lyophilized for LC–MS/MS analysis. The resulting MS/MS data were processed using the PD 2.4 search engine. Tandem mass spectra were searched against the *Homo sapiens* database concatenated with a reverse decoy database. The identified differentially expressed phosphoproteins (DEPPs) with CV values of <0.2 and the corresponding fold change scores were selected for further analyses. Using the UniProt-GOA database (http://www.ebi.ac.uk/GOA/), InterProScan software was used to annotate the GO functions of the proteins based on the protein sequence alignment method. The Kyoto Encyclopedia of Genes and Genomes (KEGG) database was used to annotate protein pathways. Then, the annotation results were mapped to the KEGG pathway database using the KEGG online tool KEGG Mapper. For each term, two-tailed Fisher's exact test was employed to determine the enrichment of the differentially expressed protein with respect to all identified proteins. Pathways with $P < 0.05$ by two-tailed Fisher's exact test were considered significantly enriched. All differentially expressed modified protein sequences were searched against the STRING database version 11.0 to identify protein–protein interactions. Chord diagrams and networks were visualized with the circlize R package and Cytoscape software.

RNA sequencing

Gastric Ly6C^{high} monocytes and moDCs from *H. pylori*-infected WT mice (14 weeks p.i.) were sorted with a fluorescence-activated cell sorter (FACS) (FACSAria III; BD Biosciences). Total RNA from FACS-sorted mouse gastric Ly6C^{high} monocytes and moDCs and total RNA from TINAGL1-stimulated (100 ng/ml, 3 h) and unstimulated Ly6C^{high} monocytes were extracted using RNeasy Micro Kits following the manufacturer's instructions. Then, the samples were sent to Guangzhou Epibiotek Co., Ltd (Guangzhou, China) for RNA sequencing. The concentration and quality of the RNA

samples were determined by a NanoDrop 2000 spectrophotometer (NanoDrop Technologies, USA), and the samples were then used to construct strand-specific (first-strand cDNA) RNA libraries with an Epi^{TM} mini longRNA-seq kit. RNA libraries were subjected to sequencing on the Illumina NovaSeq 6000 platform. Subsequently, the 150 bp paired-end reads were mapped to the reference mouse genome build mm10 by using HISAT2. The counts of reads mapped to the genome were calculated using HTSeq. The differential expression analysis presented here was performed with the DESeq2 R package. Significantly differentially expressed genes (fold change ≥ 2 and FDR < 0.05) were used to generate the PPI network, which was visualized with Cytoscape software. Gene Ontology (GO) and Kyoto Encyclopedia of Genes and Genomes (KEGG) pathway enrichment analyses were conducted with the clusterProfiler R package. Hierarchical clustering heatmaps and volcano plots were generated with the pheatmap R package and ggplot2 R package, respectively.

Statistical analysis

The results are expressed as the means ± SEMs. Student's *t* test was generally used to determine the significance of differences between two groups, but when the variances were unequal, the Mann–Whitney *U* test was used. Inflammation score data were analyzed by the Mann–Whitney *U* test. For multiple comparisons, 1-way ANOVA was used. Correlations between parameters were assessed using Pearson correlation analysis and linear regression analysis, as appropriate. SPSS statistical software (version 13.0) was used for all statistical analyses. All data were analyzed using two-tailed tests, and $P < 0.05$ was considered to indicate a statistically significant difference. Raw data from each array were analyzed using TwoClassDif.

REFERENCES

1. Hooi JKY, Lai WY, Ng WK, Suen MMY, Underwood FE, Tanyingoh D, et al. Global prevalence of *Helicobacter pylori* infection: systematic review and meta-analysis. Gastroenterology. 2017;153:420–9.
2. Polk DB, Peek RM Jr. *Helicobacter pylori*: gastric cancer and beyond. Nat Rev Cancer. 2010;10:403–14.
3. McColl KE. Clinical practice. *Helicobacter pylori* infection. N Engl J Med. 2010;362:1597–604.
4. Barcellos-Hoff MH, Lyden D, Wang TC. The evolution of the cancer niche during multistage carcinogenesis. Nat Rev Cancer. 2013;13:511–8.
5. Lv YP, Cheng P, Zhang JY, Mao FY, Teng YS, Liu YG, et al. *Helicobacter pylori*-induced matrix metallopeptidase-10 promotes gastric bacterial colonization and gastritis. Sci Adv. 2019;5:eaau6547.
6. Morey P, Pfannkuch L, Pang E, Boccellato F, Sigal M, Imai-Matsushima A, et al. *Helicobacter pylori* depletes cholesterol in gastric glands to prevent interferon gamma signaling and escape the inflammatory response. Gastroenterology. 2018;154:1391–1404.e9.
7. Mejías-Luque R, Gerhard M. Immune evasion strategies and persistence of *Helicobacter pylori*. Curr Top Microbiol Immunol. 2017;400:53–71.
8. Elinav E, Nowarski R, Thaiss CA, Hu B, Jin C, Flavell RA. Inflammation-induced cancer: crosstalk between tumours, immune cells and microorganisms. Nat Rev Cancer. 2013;13:759–71.
9. Morris AH, Kyriakides TR. Matricellular proteins and biomaterials. Matrix Biol. 2014;37:183–91.
10. Okamoto H, Imanaka-Yoshida K. Matricellular proteins: new molecular targets to prevent heart failure. Cardiovasc Ther 2012;30:e198–209.
11. Li D, Mukai K, Suzuki T, Suzuki R, Yamashita S, Mitani F, et al. Adrenocortical zonation factor 1 is a novel matricellular protein promoting integrin-mediated adhesion of adrenocortical and vascular smooth muscle cells. FEBS J. 2007;274:2506–22.
12. Shen M, Jiang YZ, Wei Y, Ell B, Sheng X, Esposito M, et al. Tinagl1 suppresses triple-negative breast cancer progression and metastasis by simultaneously inhibiting integrin/FAK and EGFR signaling. Cancer Cell. 2019;35:64–80.e7.
13. Sun L, Dong Z, Gu H, Guo Z, Yu Z. TINAGL1 promotes hepatocellular carcinogenesis through the activation of TGF-beta signaling-medicated VEGF expression. Cancer Manag Res. 2019;11:767–75.
14. Amieva M, Peek RM Jr. Pathobiology of *Helicobacter pylori*-induced gastric cancer. Gastroenterology. 2016;150:64–78.
15. Giannakis M, Chen SL, Karam SM, Engstrand L, Gordon JI. *Helicobacter pylori* evolution during progression from chronic atrophic gastritis to gastric cancer and its impact on gastric stem cells. Proc Natl Acad Sci USA 2008;105:4358–63.
16. Smythies LE, Waites KB, Lindsey JR, Harris PR, Ghiara P, Smith PD. *Helicobacter pylori*-induced mucosal inflammation is Th1 mediated and exacerbated in IL-4, but not IFN-gamma, gene-deficient mice. J Immunol. 2000;165:1022–9.
17. Bergman MP, Engering A, Smits HH, van Vliet SJ, van Bodegraven AA, Wirth HP, et al. *Helicobacter pylori* modulates the T helper cell 1/T helper cell 2 balance through phase-variable interaction between lipopolysaccharide and DC-SIGN. J Exp Med. 2004;200:979–90.
18. Shi Y, Liu XF, Zhuang Y, Zhang JY, Liu T, Yin Z, et al. *Helicobacter pylori*-induced Th17 responses modulate Th1 cell responses, benefit bacterial growth, and contribute to pathology in mice. J Immunol. 2010;184:5121512–9.
19. Zhuang Y, Cheng P, Liu XF, Peng LS, Li BS, Wang TT, et al. A pro-inflammatory role for Th22 cells in *Helicobacter pylori*-associated gastritis. Gut. 2015;64:1368–78.
20. Petrasek J, Bala S, Csak T, Lippai D, Kodys K, Menashy V, et al. IL-1 receptor antagonist ameliorates inflammasome-dependent alcoholic steatohepatitis in mice. J Clin Investig. 2012;122:3476–89.
21. Zhao Z, Hou N, Sun Y, Teng Y, Yang X. Atp4b promoter directs the expression of Cre recombinase in gastric parietal cells of transgenic mice. J Genet Genomics. 2010;37:647–52.
22. Wilson KT, Crabtree JE. Immunology of *Helicobacter pylori*: insights into the failure of the immune response and perspectives on vaccine studies. Gastroenterology. 2007;133:288–308.
23. Bimczok D, Grams JM, Stahl RD, Waites KB, Smythies LE, Smith PD. Stromal regulation of human gastric dendritic cells restricts the Th1 response to *Helicobacter pylori*. Gastroenterology. 2011;141:929–38.
24. Kao JY, Zhang M, Miller MJ, Mills JC, Wang B, Liu M, et al. *Helicobacter pylori* immune escape is mediated by dendritic cell-induced Treg skewing and Th17 suppression in mice. Gastroenterology. 2010;138:1046–54.
25. Kaparakis M, Walduck AK, Price JD, Pedersen JS, van Rooijen N, Pearse MJ, et al. Macrophages are mediators of gastritis in acute *Helicobacter pylori* infection in C57BL/6 mice. Infect Immun. 2008;76:2235–9.
26. Kurz ARM, Pruenster M, Rohwedder I, Ramadass M, Schafer K, Harrison U, et al. MST1-dependent vesicle trafficking regulates neutrophil transmigration through the vascular basement membrane. J Clin Investig. 2016;126:4125–39.
27. Van Haastert PJ, Devreotes PN. Chemotaxis: signalling the way forward. Nat Rev Mol Cell Biol. 2004;5:626–34.
28. Desgrosellier JS, Cheresh DA. Integrins in cancer: biological implications and therapeutic opportunities. Nat Rev Cancer. 2010;10:9–22.
29. Baldari CT, Lanzavecchia A, Telford JL. Immune subversion by *Helicobacter pylori*. Trends Immunol. 2005;26:199–207.
30. Ley K, Laudanna C, Cybulsky MI, Nourshargh S. Getting to the site of inflammation: the leukocyte adhesion cascade updated. Nat Rev Immunol. 2007;7:678–89.
31. Flores-Mireles AL, Walker JN, Caparon M, Hultgren SJ. Urinary tract infections: epidemiology, mechanisms of infection and treatment options. Nat Rev Microbiol. 2015;13:269–84.
32. Lu R, Goldberg MB. Bacterial exploitation of host cell signaling. Sci Transl Med. 2010;2:51ps48.
33. Shan ZG, Sun ZW, Zhao LQ, Gou Q, Chen ZF, Zhang JY, et al. Upregulation of Tubulointerstitial nephritis antigen like 1 promotes gastric cancer growth and metastasis by regulating multiple matrix metallopeptidase expression. J Gastroenterol Hepatol. 2021;36:196–203.
34. Timpl R, Sasaki T, Kostka G, Chu ML. Fibulins: a versatile family of extracellular matrix proteins. Nat Rev Mol Cell Biol. 2003;4:479–89.
35. Ham SA, Kim HJ, Kim HJ, Kang ES, Eun SY, Kim GH, et al. PPARdelta promotes wound healing by up-regulating TGF-beta1-dependent or -independent expression of extracellular matrix proteins. J Cell Mol Med. 2010;14:1747–59.
36. O'Blenes CA, Kinnear C, Rabinovitch M. Tumor necrosis factor-alpha induces fibronectin synthesis in coronary artery smooth muscle cells by a nitric oxide-dependent posttranscriptional mechanism. Circ Res. 2001;89:26–32.
37. Koch KN, Hartung ML, Urban S, Kyburz A, Bahlmann AS, Lind J, et al. Helicobacter urease-induced activation of the TLR2/NLRP3/IL-18 axis protects against asthma. J Clin Investig. 2015;125:3297–302.
38. Harris PR, Mobley HL, Perez-Perez GI, Blaser MJ, Smith PD. *Helicobacter pylori* urease is a potent stimulus of mononuclear phagocyte activation and inflammatory cytokine production. Gastroenterology. 1996;111:419–25.
39. Hynes RO. The extracellular matrix: not just pretty fibrils. Science. 2009;326:1216–9.
40. Chaudhuri O, Cooper-White J, Janmey PA, Mooney DJ, Shenoy VB. Effects of extracellular matrix viscoelasticity on cellular behaviour. Nature. 2020;584:535–46.
41. Horton ER, Byron A, Askari JA, Ng DHJ, Millon-Fremillon A, Robertson J, et al. Definition of a consensus integrin adhesome and its dynamics during adhesion complex assembly and disassembly. Nat Cell Biol. 2015;17:1577–87.
42. Calderwood DA, Campbell ID, Critchley DR. Talins and kindlins: partners in integrin-mediated adhesion. Nat Rev Mol Cell Biol. 2013;14:503–17.
43. Akhiani AA, Pappo J, Kabok Z, Schön K, Gao W, Franzén LE, et al. Protection against *Helicobacter pylori* infection following immunization is IL-12-dependent and mediated by Th1 cells. J Immunol. 2002;169:6977–84.

44. Chen L, Li B, Yang WC, He JL, Li NY, Hu J, et al. A dominant CD4(+) T-cell response to *Helicobacter pylori* reduces risk for gastric disease in humans. Gastroenterology. 2013;144:591–600.
45. Sayi A, Kohler E, Hitzler I, Arnold I, Schwendener R, Rehrauer H, et al. The CD4+ T cell-mediated IFN-gamma response to Helicobacter infection is essential for clearance and determines gastric cancer risk. J Immunol. 2009;182:7085–101.
46. Domínguez-Andrés J, Feo-Lucas L, Minguito de la Escalera M, González L, López-Bravo M, Ardavín C. Inflammatory Ly6C(high) monocytes protect against candidiasis through IL-15-Driven NK cell/neutrophil activation. Immunity. 2017;46:1059–1072.e4.
47. Roussel Y, Wilks M, Harris A, Mein C, Tabaqchali S. Evaluation of DNA extraction methods from mouse stomachs for the quantification of H. pylori by real-time PCR. J Microbiol Methods. 2005;62:71–81.
48. Mikula M, Dzwonek A, Jagusztyn-Krynicka K, Ostrowski J. Quantitative detection for low levels of *Helicobacter pylori* infection in experimentally infected mice by real-time PCR. J Microbiol Methods. 2003;55:351–9.
49. Ferrero RL, Avé P, Ndiaye D, Bambou JC, Huerre MR, Philpott DJ, et al. NF-kappaB activation during acute *Helicobacter pylori* infection in mice. Infect Immun. 2008;76:551–61.

ACKNOWLEDGEMENTS

This work was supported by grants from the National Natural Science Foundation of China (82070578, 81870394, 82000530 and 81670510), Chongqing Natural Science Fund for Distinguished Young Scholars (cstc2019jcyjjqX0003), Science Innovation Capacity Promotion Project of Army Medical University (2019XQY03) and National Key Research and Development Program of China (2016YFC1302200) and Collaborative Innovation Center of Chinese Ministry of Education (2020–39).

AUTHOR CONTRIBUTIONS

All listed authors participated meaningfully in the study, and they have seen this manuscript and approved its submission. YZ designed the study. YZ and YST performed the research, analyzed the data, and wrote the draft of the article. WC, QMZ, RX and JYX revised the manuscript. YST, RX, JYX, PW, WYC, ZGS, ZBY, FYM, PC, LSP, JYZ and WQT performed the research and collected data. QMZ, RX, JYX, SMY and YLZ contributed reagents and human clinical samples.

COMPETING INTERESTS

The authors declare no competing interests.

ADDITIONAL INFORMATION

Supplementary information The online version contains supplementary material available at https://doi.org/10.1038/s41423-023-01055-4.

Correspondence and requests for materials should be addressed to Quanming Zou or Yuan Zhuang.